

Review

Crystallization in Fluidized Bed Reactors: From Fundamental Knowledge to Full-Scale Applications

Marcelo Martins Seckler 

Department of Chemical Engineering, Polytechnic School, University of São Paulo, São Paulo 05508-010, Brazil; marcelo.seckler@usp.br; Tel.: +55-11-9996-35142

Abstract: A review is presented on fifty years of research on crystallization in fluidized bed reactors (FBRs). FBRs are suitable for recovery of slightly soluble compounds from aqueous solutions, as it yields large, millimeter sized particles, which are suitable for reuse and permits low liquid residence times in the timescale of minutes. Full-scale applications for water softening have been applied since the 1980s, and since then, new applications have been developed or are in development for recovery of phosphorus, magnesium, fluoride, metals, sulfate, and boron. Process integration with membrane, adsorption, and biological processes have led to improved processes and environmental indicators. Recently, novel FBR concepts have been proposed, such as the aerated FBR for chemical-free precipitation of calcium carbonate, the seedless FBR to yield pure particulate products, a circulating FBR for economic recovery and extended use of seeds, as well as coupled FBRs for separation of chiral compounds and FBRs in precipitation with supercritical fluids. Advances are reported in the understanding of elementary phenomena in FBRs and on mathematical models for fluid dynamics, precipitation kinetics, and FBR systems. Their role is highlighted for process understanding, optimization and control at bench to full-scale. Future challenges are discussed.

Keywords: fluidized bed reactor; homogeneous granulation; crystallization from solutions; precipitation; wastewater treatment; water softening; phosphorus removal; struvite; chiral separations



Citation: Seckler, M.M. Crystallization in Fluidized Bed Reactors: From Fundamental Knowledge to Full-Scale Applications. *Crystals* **2022**, *12*, 1541. <https://doi.org/10.3390/cryst12111541>

Academic Editors: Heike Lorenz, Alison Emslie Lewis, Erik Temmel and Jens-Petter Andreassen

Received: 13 August 2022

Accepted: 21 October 2022

Published: 28 October 2022

Publisher's Note: MDPI stays neutral with regard to jurisdictional claims in published maps and institutional affiliations.



Copyright: © 2022 by the author. Licensee MDPI, Basel, Switzerland. This article is an open access article distributed under the terms and conditions of the Creative Commons Attribution (CC BY) license (<https://creativecommons.org/licenses/by/4.0/>).

1. Introduction

Industrial crystallization from solutions is applied as a separation operation or as a means of synthesizing particulate products. Four crystallization methods exist, depending on how the solution interacts with its environment to promote the formation of the solid phase: cooling, evaporative, antisolvent and chemical reaction crystallization. The choice of the crystallization method is primarily based on thermodynamics of multiphase systems [1], meaning the solubility of the crystallizing compound plays a dominant role. Moderately and highly soluble compounds are preferably processed by either cooling or evaporative crystallization because respectively a high yield and a low energy consumption are feasible. Unacceptably low yields would result for slightly soluble compounds, so for this class of compounds either chemical reaction (precipitation) or antisolvent crystallization is applied. The latter finds use only when high valued compounds are involved, as the cost of separating and recycling the antisolvent is high, so most slightly soluble compounds are processed by chemical reaction crystallization.

Precipitation equipment usually involves rapid mixing of the reactants (timescale of seconds or lower) followed by a long period (timescale of hours) when particles are allowed to develop until they meet requirements for downstream separation from the liquid. The rapid mixing step takes place either in a static mixing device or in a high turbulence zone within the crystallizer. The crystallizer may be a gently stirred tank or a static vessel. The logic behind this process arrangement is related to the kinetics of elementary phenomena of crystallization of slightly soluble compounds. In the mixing step fast primary nucleation (timescales $\ll 1$ s) and slow crystal growth (typically 10^{-8} to 10^{-10} ms $^{-1}$) take place,

leading to particles in the nanometer to micrometer size ranges. In the crystallizer, such small particles ripen, i.e., they recrystallize, often as a different polymorph, and form large settleable agglomerates. Such agglomerates are difficult to dewater and retain impurities originally present either on their surface or in entrapped solution.

In fluidized bed reactors, the undesirable processing and quality issues of nanometer- and micrometer-sized particles are circumvented by the introduction of large, millimeter-sized seeds in fluidization. Precipitates are either formed directly upon the seeds or formed in solution and subsequently adhere to the seeds. Due to its large particle size, the product may be easily separated from the solution while retaining little moisture. The precipitate forms an important proportion of particulate, so economic recovery of the material is often possible. The liquid residence time is of only a few minutes, so the process is suitable for treatment of large streams.

An important issue in FBR design is the need to maximize retention of the precipitate on the seeds, thus minimizing solute loss as fine particles with the exiting solution. Much like in other precipitation options, FBR process design depends on specific features of each crystallizing system. Early industrial applications of FBRs were based on calcium carbonate crystallization for water softening [2,3], in calcium phosphate precipitation of phosphorus removal from domestic wastewaters [4,5] and in metal salts precipitation for heavy metal removal from industrial wastewaters [6,7]. Full-scale experiences have also been developed with an improved design, the circulating FBR, for softening of industrial water [8] and drinking water [9]. In the last decade, the interest in the topic has much increased, as Figure 1 illustrates. A few reviews have been done on specific applications of FBRs, such as in water softening [10,11] and phosphorus removal from waste streams by struvite crystallization [12,13]. An extensive and comprehensive review on FBRs has been published recently [14]. In this contribution, the fundamentals of the processes and process modeling work will be presented first. Then a range of applications for FBRs in the classic configuration as briefly explained above will be explored. Next, it will be shown how FBRs may be integrated with other unit operations to yield solutions to specific separation problems. Improved FBR concepts that have been proposed in recent years will be highlighted. Finally, challenges for the future will be discussed. Compared to previous publications, process fundamentals are covered in more depth, whereas integration of FBRs with other unit operations and improved reactor design concepts are new, so the present contribution offers a fresh improved cross section of FBR technology.

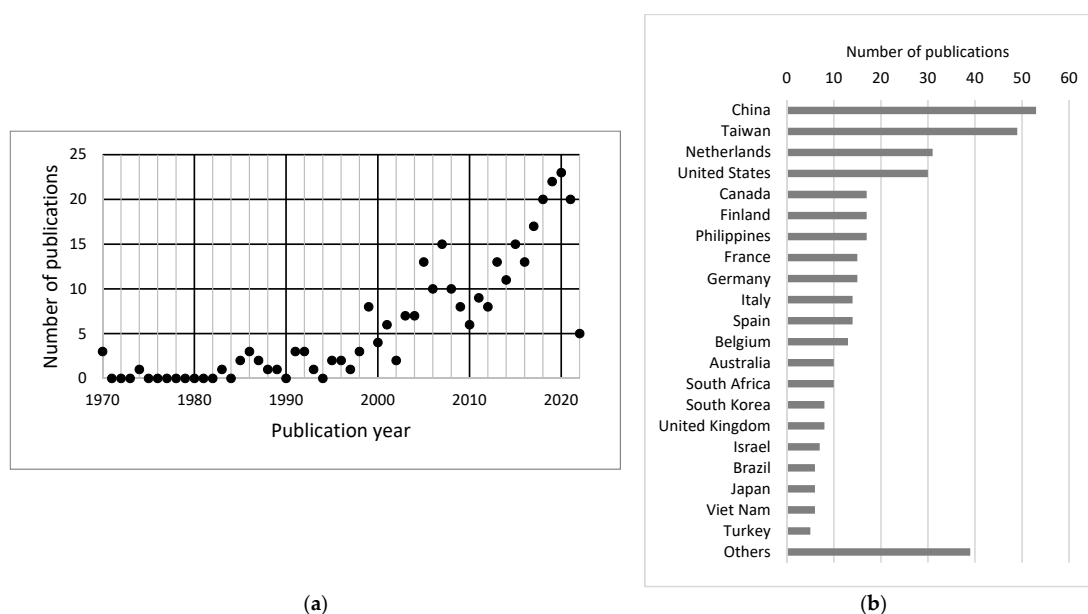


Figure 1. Number of peer reviewed publications by year (a) and by country (b). Source: Scopus, August 2022.

2. Fundamentals of FBRs and Mathematical Modeling

2.1. Main Features of FBRs and Performance Indicators

FBRs are used to separate a target compound from a liquid stream by chemical reaction crystallization. In its classic configuration (Figure 2a), reactants are mixed with the stream at the bottom of a fluidized bed. The bed is fed with seeds of a suitable size both for fluidization and for easy separation from the liquid downstream from the FBR. The seeds composition is often different from the crystallizing compound. Crystallization of the target compound takes place either directly upon the seed particles or in solution. In the latter case, most of the freshly formed precipitate adheres to the seeds. Two indicators conveniently characterize FBR performance (Figure 2b). The conversion χ is the proportion of the incoming target compound that converts to the solid phase and the recovery η gives the proportion of the incoming target compound that is retained in the seeds. Consequently, the target compound not retained in the seeds leave the system either in solution with mass fraction $1 - \chi$ or as fine particles with mass fraction $\chi - \eta$. It is desired to attain the highest possible conversion and a recovery that approaches the conversion, that is, most of the converted compound attaches to the grains. The conversion is controlled by the amount of chemicals added. Since FBRs are applied for low solubility compounds, conversions approaching 1.0 are feasible, but in some cases lower values result because a supersaturated solution leaves the crystallizer or because the formation of fines is minimized for a condition of partial conversion. Terminology in the literature is sometimes confusing, the terms removal, efficiency, crystal efficiency, granulation, among others, are used to mean either recovery or conversion. When the seeds are of the same composition as the crystallizing compound, or in case of an unseeded FBR, the term homogeneous FBR or homogeneous granulation FBR are commonly used. Grown seeds are usually called pellets, grains or simply particles.

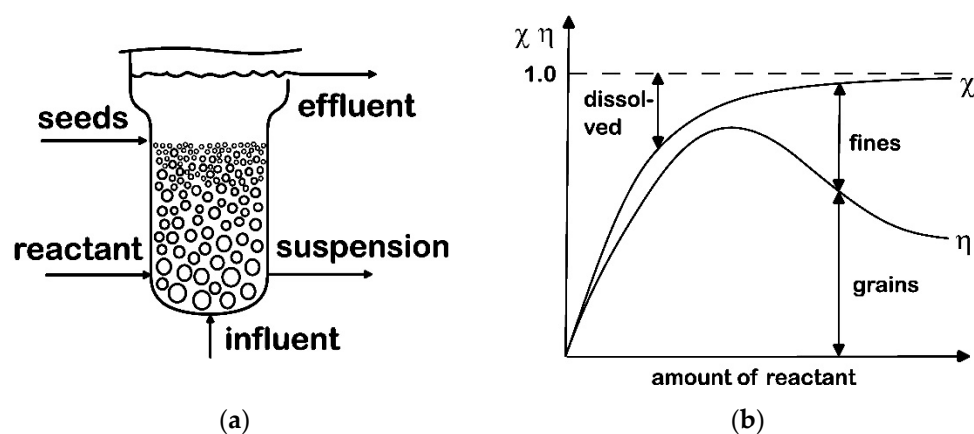


Figure 2. Fluidized bed reactor (a) and the performance indicators conversion χ and recovery η (b).

2.2. Elementary Processes of Crystallization

The first step in precipitation is the generation of supersaturation by rapid mixing of reactants with the influent at the lower part of the FBR. Two limiting behaviors may be distinguished with respect to the genesis of particle formation in FBRs depending on the supersaturation in the region where reactants are mixed and the metastable zone width of the solution. In the first one, the local supersaturation falls within the metastable zone width, so the main elementary process in the FBR is crystal growth upon the grains, possibly associated with epitaxial growth. This behavior is approached in practice for crystallization of calcium carbonate [15,16]. As an example, Figure 3 shows calcite crystals in a pellet from a full-scale reactor. In the second type of behavior, the local supersaturation exceeds the metastable zone, and primary heterogeneous nucleation takes place in solution at the bottom of the bed, so recovery occurs by aggregation of the resulting fine particles with the grains as they ascend within the bed. This behavior is usually found for compounds

with extremely low solubility, such as amorphous calcium phosphate [17], nickel sulfide and copper sulfide [18], and nickel/cobalt sulfide mixtures [19]. Figure 4 illustrates this mechanism by the measurement of the fine particles' concentration profile in the fluidized bed: the fines are formed at the bottom and subsequently disappear as they aggregate upon the grains as they ascend. Struvite appears to exhibit intermediate behavior [20,21]. Fine particles may also be created by grains abrasion, particularly for seeds of large size or in regions of high turbulence, such as in the zone of reactants mixing. Abrasion may be easily noticed by a rounded shape and smooth surface of the grains, as illustrated in Figure 5a for grains collected from the bottom of a FBR. Figure 5b shows that grains at the top of the same bed, where turbulence is lower. In the absence of abrasion, particles display a rough, irregular surface. During start up, when the bed is filled with bare seeds, heterogeneous nucleation of the target compound upon the seeds surface controls recovery, which is lower than at steady operation. Such induction period usually last a few minutes [22] to a few hours [17].

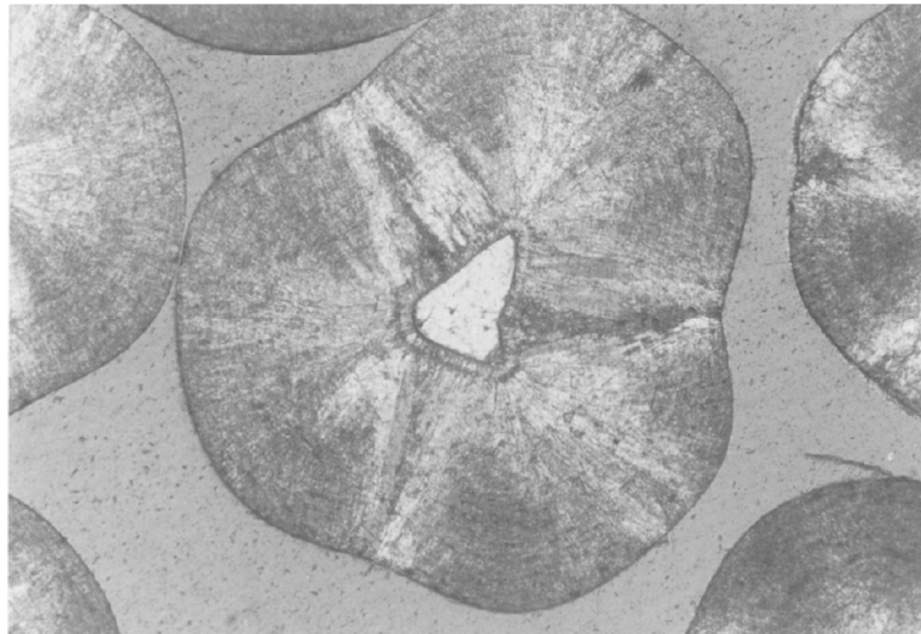


Figure 3. Photomicrograph in thin section of a pellet from a full-scale FBR. The small, clear particle at the center is the seed. The rest of the particle are calcite crystals displaying concentric layering and stellate clusters of coarser calcite. Field of view: 4 mm. Source [16].

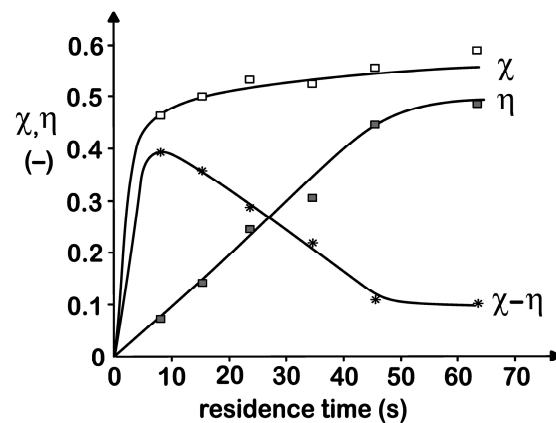


Figure 4. Conversion (χ), recovery (η), and fines ($\chi - \eta$) along bed height (expressed as residence time in the bed), suggesting that fines are formed at the bottom and subsequently adhere to the grains. Source: [23].

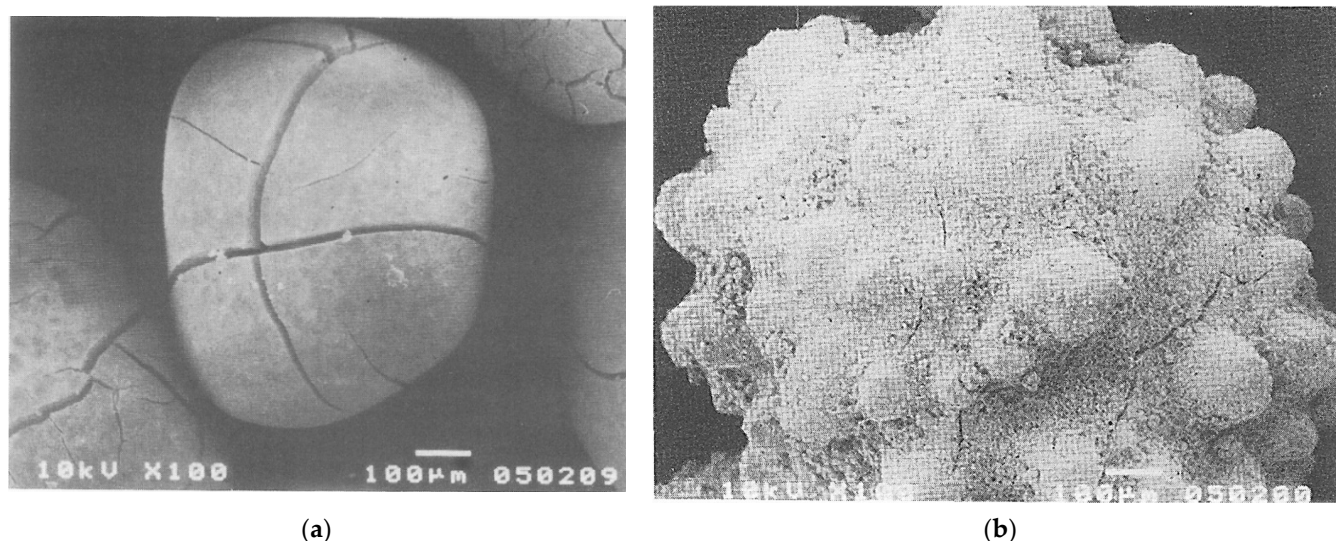


Figure 5. SEM view of (a) a highly abraded grain collected from the bottom of a FBR and (b) a non-abraded grain collected from the top of the same bed. The compound is amorphous calcium phosphate. Source: [24].

The specific surface area of the particles, expressed in m^2 per m^3 fluidized bed is an important parameter in FBR design because a high value allows fast consumption of supersaturation that would otherwise promote undesired primary nucleation in solution as opposed to crystal growth upon the seed grains. Additionally, a high superficial velocity implies efficient use of the reactor volume for crystallization.

Mathematical models for elementary phenomena of a FBR are summarized in Table 1. Models that consider thermodynamic equilibrium and chemical speciation in solution are useful for establishing conditions for crystallization of the desired target compound [25] without coprecipitation of unwanted compounds [24] and to assess the influence of ligands on precipitation [26]. They also help to determine whether effluents leave the crystallizer as a supersaturated solution [27]. Particle growth and crystal growth kinetics in FBRs have been determined which are helpful for design, be it a kinetic expression for a two-step crystal growth as function of supersaturation [28,29] or an empirical correlation for the particle growth rate that includes dependencies for supersaturation, particle size and superficial velocity [30,31]. A kinetic model for aggregation of amorphous calcium phosphate allowed an improved understanding of the FBR operation [17]. A CFD-based population balance model has been developed to represent the nucleation and crystal growth at the bottom of a FBR [32]. The model predicts local supersaturations and particle sizes for calcium phosphate.

Table 1. Mathematical models for elementary phenomena in FBRs. Equilibrium: indicates that solubility, supersaturation and in some cases solution speciation are considered. Growth: indicates whether molecular crystal growth (indicated as “crystal”) or overall particle growth, which encompasses crystal growth, aggregation and abrasion (indicated as “particle”) are considered.

Crystallizing Compound	Elementary Phenomena	Authors	Year	Refs.
CaCO_3	Equilibrium, crystal growth	Hu et al.	2017	[15]
CaCO_3	Equilibrium, crystal growth	Rankin et al.	1999	[16]
Ca phosphate	Equilibrium, crystal growth, aggregation	Seckler	1994	[17]
NiS–CoS	Equilibrium, particle growth, aggregation	Lewis et al.	2006	[19]
Struvite	Equilibrium, metastable zone width, crystal growth	Bhuiyan	2008	[20]
Ca phosphate	Equilibrium	Seckler et al.	1996	[24]

Table 1. Cont.

Crystallizing Compound	Elementary Phenomena	Authors	Year	Refs.
Ca phosphate	Equilibrium	Montastruc et al.	2003	[25]
Struvite	Equilibrium	Iqbal et al.	2008	[26]
Struvite	Equilibrium	Xu et al.	2019	[27]
CaCO ₃	Equilibrium, crystal growth	Tai et al.	1999	[28,29]
CaF ₂	Equilibrium, particle growth	Aldaco et al.	2007	[30,31]
Ca phosphate	Equilibrium, nucleation, crystal growth, macromixing	Seckler et al.	1995	[32]

2.3. Liquid Solid Fluidization

Liquid solid fluidization is encountered in elutriation, leaching, crystallization of moderately soluble compounds, etc. Generally, a homogeneous bed of increasing height develops for superficial velocity's varying between the minimum fluidization velocity and the terminal falling velocity of the particles [33]. Table 2 summarizes mathematical models for fluidization in FBRs. Kramer et al. [34] have compared several models for predicting the voidage of monodispersed calcite particles to a wide range of experimental conditions. The best fitting was found for their explicit model of the form $\varepsilon = \varepsilon(\text{Re}, \text{Fr})$, with ε , Re and Fr representing the bed voidage, the Reynolds and the Froude number, respectively. They have also suggested that such an explicit, simple model is the most suitable approach for monitoring and control of full-scale processes. Ye et al. [35] have used a CFD model to show that particles recirculate within the bed.

Table 2. Mathematical models for fluidization in FBRs. ¹ Dimension 0D indicates that voidage is calculated in a homogeneous bed; 1D and 3D indicate particle segregation in one dimension (bed height) and three dimensions, respectively. ² Particle segregation indicates whether particles are homogeneously distributed within the FBR, segregated by size, or by both size and density.

Crystallizing Compound	Dimensions ¹	Particle Segregation ²	Authors	Year	Reference
CaCO ₃	0D	None	Kramer et al.	2020	[34]
Struvite	3D	None	Ye et al.	2017	[35]
	1D	Size	Toyokura et al.	1973	[36]
NaBO ₃ ·4H ₂ O	1D	Size	Frances et al.	1994	[37]
	1D	Size	Shiau et al.	2001	[38]
	3D	Size	Al-Rashed et al.	2009	[39]
	3D	Size	Al-Rashed et al.	2013	[40]
Struvite	3D	Size	Rahaman et al.	2018	[41]
Ca phosphate	1D	Size and density	Seckler	1994	[17]
CaCO ₃	1D	Size and density	van Schagen et al.	2008	[42]
Enantiomers	3D	Size	Kerst et al.	2017	[43]

Particles of different sizes usually segregate, larger particles occupying lower portions of the fluidized bed. Segregation however is not perfect, so polydisperse materials occupy each axial position within the bed. This behavior has been addressed by Toyokura et al. [36] with an axial-dispersion model, whereas Frances et al. [37] and Shiau et al. [38] have used a mixed-tank in series approach. Al-Rashed et al. [39,40] have indicated with CFD simulations that the voidage and particle size changes both with axial and radial position within Oslo-fluidized bed crystallizers. In addition, upon scaleup at constant superficial velocity, voidage decreases due to cessation of fluid circulation flows. In a cylindrical bench

scale crystallizer, both CFD and experiments have yielded a size-segregated bed with little dispersion [41].

If particle size and density vary, as is the case when the seeds and the crystallizing compound have different densities, stratification is more complex. Kennedy and Bretton [44] have considered that the driving force for segregation is the difference between the slip velocity of a given particle and the upward fluid velocity and included an axial dispersion coefficient that counteracts segregation. This basic idea has been pursued later with improvements in solution and accuracy [45,46]. Gibilaro et al. [47] established that the particles distribute in the bed in such a way that the potential energy is minimized. Seckler [17] has developed a mathematical model using this concept to adequately describe the composition and size of particles as functions of the height in a bench scale bed with sand pellets covered with amorphous calcium phosphate. Van Schagen et al. [42] have noticed that fluidization models do not accurately represent experimental data for calcium carbonate crystallization in pilot and industrial units. They have assumed that particles which size and density promote a higher pressure drop occupy a lower position in the bed. They have concluded that the calibrated Richardson Zaki model is the most accurate. Using this model, operational constraints have been established in terms of minimal and maximal pellet size at the bottom, for given superficial velocity and temperature. They have found that such operational constraints are often violated in practice, so they have recommended to use the model and to measure pressure drop at the bottom of the bed, instead of pressure drop of the total bed, as is usual.

2.4. Mathematical Models for the FBR Process

Models that describe the FBR process are summarized in Table 3. They combine fluid dynamics, mass balances, equilibrium, and crystallization kinetics, with time and special coordinates as independent variables. Models that describe the recovery and the grain size as functions of time and bed height have been proposed for crystallization of calcium carbonate [48], struvite [49–51], potassium struvite [52], calcium phosphate [53,54], gypsum [55,56], and tetrahydrate sodium perborate [37]. Precipitation is often modelled with the surface-controlled crystal growth rate with an expression of the type,

$$G = k_g(S - 1)^g \quad (1)$$

where S is the supersaturation ratio, $S = c/c_{eq}$, with c and c_{eq} ($\text{kg}\cdot\text{m}^{-3}$) as the active component concentrations in the supersaturated solution and in equilibrium, respectively, k_g and g are fit parameters, the latter being the growth order. Sometimes diffusion is considered the controlling mechanism for particle growth, so Equation (1) takes the form,

$$G = k_d(c - c_{eq}) \quad (2)$$

The mass transfer coefficient k_d has both been determined experimentally in a FBR [20] or estimated with semi-empirical correlations, such as the Froessling equation that relates the numbers of Sherwood, Reynolds and Schmidt [28]:

$$Sh = 0.6Re^{\frac{1}{2}}Sc^{\frac{1}{3}} \quad (3)$$

Most often, particle abrasion and fines aggregation upon the grains are lumped into Equation (1), whereas primary nucleation is neglected. The removal of the active component from solution relates to the particle (overall) growth rate G with the mass balance for a horizontal slice of the bed,

$$\frac{dc}{dh} \sim \rho_{solid}Gu^{-1}dA \quad (4)$$

where h (m) is the bed height, dA (m^2) is the interfacial area of the grains, u ($\text{m}\cdot\text{s}^{-1}$) is the superficial velocity and ρ_{solid} is the solid density ($\text{kg}\cdot\text{m}^{-3}$). The value of dA is derived from a fluid dynamics model, for which a fully segregated bed is the most straightforward option.

The calculations are performed for each differential slice of the bed at each time interval starting at the moment of seeds addition, implying that G , c and A are functions of h and t , $G = G(h,t)$, $c = c(h,t)$, $A = A(h,t)$. The recovery after a certain period of operation is calculated from the value of c at the top of the bed, whereas the grains size $L = L(h,t)$ is calculated from the seeds size and integrating $G(h,t)$ with time for each horizontal slice. Fines leaving the bed from the top are neglected. This type of model is useful for design when complemented by experimental data on bench or pilot-scale FBRs, as it is restricted to an operating range in which primary nucleation is negligible. It is suitable for systems in which recovery largely depends on crystal growth, such as in calcium carbonate and gypsum-based systems, but not for systems in which primary nucleation in solution and subsequent aggregation with the grains are the dominant phenomena, such as calcium phosphates.

Table 3. Mathematical models for FBRs. ¹ Growth: indicates whether molecular crystal growth (indicated as “crystal”) or overall particle growth, which encompasses crystal growth, aggregation and abrasion (indicated as “particle”) are considered. ² Dimensions 0D indicates that the independent variables are respectively particle size (L) and time (t); 1D indicates that they are L , t , and the bed height; 3D relates to models in L , t , and the three spatial dimensions. ³ Particle segregation indicates whether particles are homogeneously distributed within the FBR or segregated by size, or by both size and density.

Crystallizing Compound	Growth ¹	Dimensions ²	Particle Segregation ³	Other Phenomena	Authors	Year	References
Struvite	Particle	0D	None	aggregation	Bhuiyan et al.	2008	[20]
CaCO ₃	Crystal	0D	None		Tai et al.	1999	[28]
CaCO ₃	Crystal	1D	Size and density		Van et al.	2008	[48]
Struvite	Particle	1D	Size		Rahaman et al.	2014	[49]
Struvite	Particle	1D	Size		Rahaman et al.	2008	[50]
K struvite	Crystal	1D	Size		Zhang et al.	2017	[52]
Ca phosphate	Crystal	1D	Size	Fluid mixing, aggregation	Montastruc et al.	2003 2004	[53,54]
Gypsum	Crystal	0D	None		Choi et al.	2021	[55,56]
Ca phosphate	Crystal	3D	Size	Macromixing	Seckler et al.	1995	[32]
CaCO ₃	Crystal	1D	Size and density		van Schagen et al.	2006	[57,58]
Struvite	No	3D	None	Nucleation, Macromixing	Ye et al.	2018	[59]
Struvite	Crystal	3D	Size	Macromixing	Rahaman et al.	2018	[41]
BaCO ₃	Crystal	3D	Size	Nucleation, Micromixing, aggregation	Moguel et al.	2010	[60]
CaCO ₃	Crystal	0D	None	CO ₂ stripping	Segev et al.	2013	[61]
Enantiomers	Crystal	1D	Size	Nucleation, Breakage	Mangold et al.	2017	[62]
Enantiomers	Crystal	1D	Size	Nucleation, Breakage	Gänsch et al.	2021	[63]

Van Schagen et al. [57,58] have developed a model for process control of softening in full-scale FBRs based on crystal growth rate and complete grains segregation. A nonlinear model-predictive controller determines the values of the manipulated variables to keep the pellet size and bed height within desired range under varying operational conditions. They have found optimal values for the pellet size and for the bypass ratio (part of the influent is diverted because the FBR exceeds softening specifications) while maximizing bed height (to reduce residual supersaturation). The approach has been considered robust to inaccurate measurements.

Ye et al. [59] have developed a model for a FBR in three dimensions at unsteady state. The multiphase flow was modelled with a commercial Reynolds-averaged Navier-stokes

CFD code and particle mean sizes were determined with the moments transformation of the population balance. Crystal growth and primary nucleation kinetics with the literature parameters for struvite have been adopted. Phosphorus removal at various process conditions compared favorably with bench scale experiments, and a split inlet of reactants was suggested as useful for improved control of the supersaturation. The model is useful for performance evaluation and geometry optimization of FBRs in which aggregation is not an important phenomenon. It does consider the formation of small particles in solution. Rahaman et al. [41] have also developed a CFD model for struvite crystallization and compared it to pilot experiments. Moguel et al. [60] have developed a CFD model for barium carbonate precipitation in a FBR that included micromixing limited chemical acid–base instantaneous reaction, solution speciation, phase equilibrium, and kinetics for nucleation, growth, and aggregation. The model has been compared to pilot-scale experiments.

3. Applications

3.1. Calcium Carbonate

Calcium carbonate crystallization is applied in central softening of drinking water as it reduces scaling in household appliances and surfaces and reduces the need for cleaning agents and laundry detergents. Even though the FBR process requires energy and chemicals, it has been shown to be environmentally positive from life cycle assessment [64] and from a cost benefits [65] perspective. In addition, carbon capture in the crystallized calcite and dissolution of CO₂ into the softened water offers net carbon benefits of softening. The net total carbon footprint of drinking water softening in the Netherlands is estimated to be −0.11 Mton CO₂ eq./yr. [66].

Calcium carbonate crystallization in a FBR is the first and most developed application of FBR technology. It has already received reviews in the nineties [10,11,67], as well as a recent one [14]. Pilot studies and industrial scale applications of FBRs started in the 1970s [2,3]. In the present day there are full-scale units located in the Netherlands [34,68,69], in Saudi Arabia, in the United States of America [70], and in China [8,9]. An overview of full-scale and pilot-scale applications of FBRs is given in Tables 4 and 5, respectively. A full-scale circulating FBR has been used for softening of tower water in a thermal power plant [8], where softening enabled an increase in water circulation ratio from 4.5 to 9, to reduce anti scaling additive consumption by 30% and to use the pellets in the desulfurization unit of the power plant. The same FBR design has led to improved performance of full-scale in terms of hardness removal, time interval for pellets withdrawal, and cost [9].

The process is driven by adding a base to increase the water pH to values between 9 and 11. Calcium hydroxide is often used because of its low cost and to provide calcium if carbonate is originally in excess. If calcium is in excess, some sodium carbonate may be added [71]. Pellets are mainly constituted by calcite. This was for example the case for 16 water types at eight Danish drinking water treatment plants [72]. Besides calcite, they contained impurities, such as strontium, magnesium, iron, and sodium, each contributing with up to 1.3% of the pellet mass. The influent water composition did not change the calcium carbonate mineralogy but did correlate with the concentrations of many (but not all) impurities in the pellets. Quartz sand seeding material contributed with up to 15% of the pellet mass. The grains' low specific surface area of $\leq 0.32 \text{ m}^2/\text{g}$ limits its potential use as soil amendment in agriculture [72]. In another study [71], garnet seeds were covered with calcium carbonate (97%) and magnesium hydroxide (3%). The polymorph aragonite was the main mineral in grains produced in a homogeneous (unseeded) FBR [73].

Rankin and Sutcliffe [16] have characterized the microstructure of calcite covering sand seeds in an industrial softening FBR. They have identified concentric banding inside the particles associated with perturbations in growth conditions induced by changes in pH inside the reactor. They have also found that individual “calcite crystals grow orthogonally from the surface of the seeds and in optical continuity across the concentric bands” and that “stellate clusters of larger crystals cross-cut these bands”. Consequently, crystal growth is the dominant process in particle formation, with a growth rate of the order of 0.1 mm

per day. A two-step growth model has been suggested [28], as well as semi-empirical rate laws for growth rate dependency of the supersaturation [15,74]. Most calcium and total hardness crystallize at the lowest part of the bed, within a bed height of about 1 m [8,11].

Fines lost with the effluent may result from abrasion of the pellets or from heterogeneous nucleation in solution. In a study with eight real groundwater types in a circulating FBR [71], fines were found to be predominantly calcium carbonate and magnesium carbonate particles. Fines formation could be hindered if $\text{Ca}^{2+} < 180 \text{ mg/L}$, $\text{Mg}^{2+} < 70 \text{ mg/L}$, and $\text{pH} < 11$.

Mathematical models have been developed for several aspects of a softening FBR, such as fluidization; see Section 2 in this manuscript.

3.2. Calcium Phosphates

Calcium phosphates crystallization is mostly applied to remove phosphate from wastewaters that would otherwise cause eutrophication of surface waters. Early studies on calcium phosphate precipitation in a FBR have been developed from bench to industrial scale [4,5,75]. The calcium phosphate compound formed in FBRs is an amorphous phase that may be represented by the chemical formula $\text{Ca}_3(\text{PO}_4)_2$ [23]. The process is controlled by aggregation of primary particles upon the seeds [23], so P recovery is improved by using multiple reactant inlet points to avoid high local supersaturations and to enhance aggregation [76]. A poorly crystalline hydroxyapatite is formed sometimes [77], probably by recrystallization of amorphous calcium phosphate at a low supersaturation and a long residence time [78]. A commonly used seed material is quartz sand, which provides an inert surface for phosphorus nucleation and retention in the bed. Seeding with MgO grains is more effective as it produces alkalinity near the grain surface, which promotes precipitation of carbonates and phosphates upon them [77]. Many wastewaters contain calcium and carbonate, which tend to co-precipitate with calcium phosphate, as the rise in pH is the driving force for precipitation of both compounds. The effect of carbonate on P recovery is controversial. Not only has a positive effect been found [79], but also a negative one [24]. Magnesium has been found to suppresses undesirable CaCO_3 coprecipitation [77]. Magnesium may also precipitate as $\text{Mg}_3(\text{PO}_4)_2 \cdot 22\text{H}_2\text{O}$, yielding a feasible process for phosphorus removal for waters with a low calcium content ($\text{Ca/P} < 0.8 \text{ mol mol}^{-1}$) [24]. Fluorapatite, $\text{Ca}_{10}(\text{PO}_4)_6\text{F}_2$, may also precipitate in alkaline conditions upon phosphate rock and calcite seed particles [78]. Optimal conditions for phosphorus and fluoride removal are an upflow velocity of $0.12 \text{ m} \cdot \text{min}^{-1}$, Ca:P:F molar ratio of 10:4:1.

A thermodynamic model for calcium phosphates precipitation for FBR conditions shows that for pH values below 7.3 dicalcium phosphate is formed, for higher pH values amorphous calcium phosphate develops [25]. Equilibrium modeling has also been applied to select conditions where coprecipitation of unwanted salts are avoided [24]. Such models offer possibilities for improving recovery, increasing product purity, and reducing effluent pH.

3.3. Struvite

Struvite ($\text{NH}_4\text{MgPO}_4 \cdot 6\text{H}_2\text{O}$) crystallization has received much attention in the context of wastewater treatment because it offers the possibility of simultaneously removing two commonly encountered nutrients, phosphorus and nitrogen. Bench scale studies have started in the turn of the millennium [80–84], and since then, pilot studies [26,85–91] as well as full-scale applications have been reported [92–94]. A FBR process is nowadays explored commercially with the tradename Ostar[®] [95].

Siciliano et al. [96] have recently published an extensive review that includes struvite crystallization in FBRs. The treated wastewater should not contain less than $\sim 50 \text{ mg P/L}$, which roughly corresponds to the solubility of struvite. For this reason, this process has been studied for wastewaters containing high concentration of nutrients, such as swine [27,51,86,97–101] and chicken [102] wastewater, sludge lagoon wastewater [82], wastewater from vacuum toilet systems [103], wastewaters from industrial processes that

use phosphoric acid, such as in the manufacture of electronics [104] and activated carbon [88], and wastewater from the dairy industry [105]. For effluents with low P content, it is possible to treat them with phosphorus-accumulating microorganisms, which subsequently release P in a higher concentration suitable for struvite crystallization, as is the case for supernatants from anaerobic digestion processes [20,49,50,80,83,84,89,90,94,106–108]. If the wastewater contains potassium, such as in source-separated urine, it is convenient to have potassium struvite ($\text{KMgPO}_4 \cdot 6\text{H}_2\text{O}$) as the target compound [52,87,109].

In the classic FBR configuration, phosphorus removal values above 90% are commonly found. Residence times vary within the range of a few minutes to a few hours due to recirculation of the effluent. Superficial velocities are generally within the range of 1 to 4 $\text{m} \cdot \text{min}^{-1}$. Alkaline pH values, typically 8 to 10, are required to shift the chemical equilibrium of the reactions involving H^+ , H_3PO_4 , H_2PO_4^- , HPO_4^{2-} and PO_4^{3-} toward the latter species, which make up the crystal lattice of struvite. Magnesium is added stoichiometrically or in some excess, i.e., Mg:P molar ratios of one or slightly above it, to assure low concentration of the target compounds N and P. Seeding may be performed with struvite itself [104], with sand [81,110] or calcium phosphate [111], to yield a sub-millimetric particulate struvite product. Many process variations have been proposed to improve recovery, reduce chemicals' consumption, improve the quality of the struvite product, and reduce the residence time. They are addressed in Sections 4 and 5 in this manuscript.

Bhuiygan et al. [20] have studied the kinetics of struvite crystallization for conditions relevant for FBRs. They have determined the induction time as a function of supersaturation and the metastable zone width. Additionally, crystal growth rate kinetics have been determined in a bench scale fluidized bed. They have concluded that nucleation may be triggered at the bottom section of the bed and that the fresh crystals ascend to the top section, where a lower relative velocity should be provided so they do not escape the bed. As they grow, they gradually descend to lower portions of the bed. Nucleation and crystal growth rates have been determined in a mixed suspension crystallizer [112]. Ye et al. [113] have analyzed the morphology of struvite aggregates formed in unseeded jar tests. They have found that large, compact, mechanically strong aggregates are formed at a low phosphorus concentration and mild alkalinity. Fromberg and collaborators [21] have experimentally determined induction times and zeta potentials in struvite crystallization. They have concluded that a high recovery in FBRs might be attained by keeping a low supersaturation, because it results in low zeta potential values that favor agglomeration of primary nucleated struvite crystals upon the seeds. Consistent with these predictions, Gosh and collaborators [114] have experimentally determined that struvite recovery increases as the supersaturation decreases. Fang et al. [115] have conducted batchwise precipitation of struvite to determine its settleability, which is important for fines formation in FBRs. Ostwald ripening of struvite is suggested to explain why larger crystals develop at higher temperatures.

3.4. Other Phosphates

Besides calcium phosphate and struvite, other phosphates have been crystallized in FBRs. Barium hydrogen phosphate, BaHPO_4 , and barium oxide, BaO , have been formed [116]. A Ba recovery of 98% was achieved at a pH of 8.5, a Ba/P molar ratio of one, and a superficial velocity of 0.46 $\text{m} \cdot \text{min}^{-1}$. The addition of seeds had no effect on Ba recovery. Shih and collaborators [117] have added several alkaline earth metals but no seeds to remove phosphate from an electronics manufacturing wastewater with a high inlet P concentration of 100 ppm. It has been found that the pH determines the pseudopolymorph formed: a mixture of monetite (CaHPO_4) and brushite ($\text{CaHPO}_4 \cdot 2\text{H}_2\text{O}$) is recovered at pH 4.5, whereas hydroxyapatite ($\text{Ca}_5(\text{PO}_4)_3(\text{OH})$) is formed at pH 7.5. Strontium and barium hydrogen phosphate (SrHPO_4 and BaHPO_4) crystallize at pH 4, whereas $\text{Sr}_5(\text{PO}_4)_3(\text{OH})$ and $\text{Ba}_5(\text{PO}_4)_3(\text{OH})$ are produced at pH 8. Magnesium phosphate crystallizes as newberite (MgHPO_4) and bobierrite ($\text{Mg}_3(\text{PO}_4)_2$). Cobalt precipitates as $\text{Co}_3(\text{PO}_4)_2 \cdot 8\text{H}_2\text{O}$ and a mixture of cobalt and nickel, with the latter crystallizing as $\text{Cu}_2(\text{PO}_4)\text{OH}$, by mixing two

wastewaters from the semiconductor industry [118], one containing cobalt, the other one phosphate. EDTA and citrate ions, which are commonly found in these wastewaters, reduce recovery substantially.

3.5. Fluoride

Effluents containing fluoride are generated in fertilizer production (580–1680 ppm), optoelectronic and aluminum electroplating (100–6500 ppm), in municipal sewage treatment plants (5000–10,000 ppm), in aluminum trifluoride manufacture, and in groundwater (references given in [119]). The target compound chosen depends on the effluent specification in terms of fluoride concentration. Fluorite (CaF_2) is convenient for many industrial wastes as it yields effluents with ~ 10 ppm F^- at room temperature or ~ 5 ppm F^- at 80°C . Cryolite (Na_3AlF_6) is sometimes considered as an intermediate step as it yields effluents with concentrations an order of magnitude higher. Fluorapatite has been considered for even lower effluent concentrations of about 2 ppm, such as for groundwater treatment aiming at drinking water supply [78,120]. A life cycle assessment study shows that fluorite (CaF_2) precipitation in a FBR compares favorably with precipitation in mixed tanks [121].

Calcium fluoride precipitates upon heterogeneous seeds by addition of a calcium source (calcium chloride or calcium hydroxide) at pH values in the range of 3 to 12. A neutral pH is preferred to avoid coprecipitation of compounds, such as phosphate and carbonate, which would take place at an alkaline pH. As an example, a FBR for calcium fluoride precipitation has been applied for wastewater from a rare-earth smelting wastewater [22]. Using silica sand as seeds, recoveries above 90% have been achieved with a particle size of about 1.5 mm. The superficial velocity was $2.4\text{ m}\cdot\text{min}^{-1}$, the recycle ratio of the effluent was 0.8.

The formation of CaF_2 fines is sensitive to supersaturation [122]. It has been largely avoided by keeping the saturation index (defined as the logarithm of the ratio of ion product to solubility product) at the bottom of the reactor below 3.5 [123]. Alternatively, it has been suggested to limit the supersaturation by using fluoride concentrations lower than 150 ppm at the bottom of the FBR after mixing of reactants [124]. If the influent concentration is higher, a recirculation stream may be applied, provided that fines in this stream are removed by filtration. If reintroduced into the FBR, the fines reduce recovery because they do not aggregate with the pellets, instead they promote crystallization of CaF_2 onto their surfaces [122]. Calcium fluoride precipitation has been applied even for high influent concentrations of 5.000 ppm F^- [119]. In such cases, another option, which has been applied at a pilot-scale, is to use two FBRs in a series, the first one recovers 70% of the fluorite as cryolite, the latter separates 90% of the remaining fluoride as its calcium salt [125]. Cryolite is formed upon addition of sodium hydroxide and aluminum hydroxide at pH values in the range of 2.5 to 7 [125].

Silica sand is suitable as a substrate for CaF_2 crystallization but not for economic use of the pellets in HF production, as part of the fluoride is lost as silicon tetrafluoride gas. Consequently, crystallization upon calcite grains has been proposed [124]. If conducted at an adequate pH, the seeds partly dissolve to form additional CaF_2 and release CO_2 . After 230 h operation, it is possible to recover pellets containing 97% CaF_2 and only 3% calcite. This process has yielded F^- recoveries of 70 to 80% [126].

Table 4. Full-scale investigations with FBRs.

Crystallizing Compound	Wastewater Source	Inlet Concentration (mM)	Superficial Velocity (m/min)	Bed Diameter (cm)	Recovery (%)	Seed Material	Grain Size (mm)	Note	Author Year	Refs.
CaCO ₃	thermal power plant	0.4	0.83–1.8	240	0.5	garnet	0.1–0.3	(2)	Hu et al., 2019	[8]
CaCO ₃	drinking water	1.9	1.0–1.7	160	0.9	garnet	0.53	(2)	Hu et al., 2018	[9]
CaCO ₃	drinking water	n.a.	n.a.	n.a.	n.a.	n.a.	n.a.		several	[34,48,57,68,69]
CaCO ₃	drinking water	n.a.	1.0–1.7	260	n.a.	garnet	1.2		van Schagen et al., 2008	[58]
CaCO ₃	inland desalination	n.a.	n.a.	n.a.	n.a.	n.a.	n.a.		van Houwelingen et al., 2010	[70]
Ca phosphate	domestic, aerobic	0.16–0.32	0.67	250	77%	quartz	0.4		Seckler et al., 1990	[5]
Struvite	domestic, anaerobic	n.a.	n.a.	n.a.	n.a.	n.a.	0.5–1.0		Ueno et al., 2001	[92]
Struvite	domestic, anaerobic	1.1–2.2	1.3–2.6 min (1)	n.a.	77% P	struvite	0.5–5.0	(1)	Crutchik et al., 2017	[93]
Struvite	domestic, anaerobic	1.6	n.a.	1–8 m ³ /h (6)	60–70% P	quartz	0.2–0.35	(6)	Battistoni et al., 2006	[94]
Struvite	n.a.	n.a.	n.a.	n.a.	n.a.	n.a.	n.a.		Ostara et al., 2022	[95]

¹Notes: n.a. not available, (1) hydraulic retention time, (2) circulating FBR, (6) influent flow rate.

Table 5. Pilot-scale investigations with FBRs.

Crystallizing Compound	Wastewater Source	Inlet Concentration (mM)	Superficial Velocity (m/min)	Bed Diameter (cm)	Recovery (%)	Seed Material	Grain Size (mm)	Note	Author Year	Refs.
CaCO ₃	drinking water	n.a.	0.67–1.7	30	n.a.	garnet	0.25–1.8		van Schagen et al., 2008	[42]
CaCO ₃	drinking water	10–400	1.8	60	70	garnet	1	(2)	Hu et al., 2021	[71]
CaCO ₃	drinking water	3.2–6.1	1.3	9.9		quartz	1.0–1.2		Tang et al., 2019	[72]
CaCO ₃	desalination	36	0.096	14	0.95	quartz	0.38 (seed)	(2)(5)	Segev et al., 2011	[127]
CaCO ₃	drinking water	7.5	7.5 h (1)	7–38	0.75	Iron oxide	0.005	(1)(3)(5)	Li et al., 2004	[128]
CaCO ₃	drinking water	n.a.	n.a.	n.a.	n.a.	n.a.	n.a.		several	[2,3,15]
CaCO ₃	agriculture, industry and drinking water	10	20 min (1)	76	0.85	tartar scale, sand		(1)(4)	Nefzi et al., 2004	[129]
CaCO ₃ , Mg Silicate	coal gasification	10–400	0.25–0.50	130	50–82%	seedless	-	(2)	Hu et al., 2021	[130]
Ca phosphate	domestic, aerobic	0.24	0.9	20	80%	quartz	0.1–0.6		van Dijk et al., 1985	[4]
Ca phosphate	n.a.	0.06–0.74	3.1 min (1)	10	80%	phosphate rock	0.31 (seed)	(1)	Hirasawa I, Toya Y., 1990	[75]
CuCO ₃ Cu(OH) ₂	chemical, mining, and plating industry	0.47–4.7	15 min (1)	10	88–96%	quartz	0.26	(1)(5)	Lv et al., 2018	[131]
Fluorite	semiconductor industry	~1	n.a.	3 m ³ /h	0.95	sand	-		van den Broeck et al., 2003	[123]
Fluorite	Fluoride industry	47–89	0.06	40–70	0.95	caco3	0.08–0.15		Jiang et al., 2017	[125]
Metal (basic) carbonates	plating and chemical industry	40–60,000 ppm metal	n.a.	10	>97%	n.a.	n.a.		Scholler et al., 1987	[7]
Struvite	domestic, anaerobic	n.a.	4	n.a.	75–85% P	n.a.	n.a.		Iqbal et al., 2008	[26]
Struvite	domestic, anaerobic	n.a.	n.a.	n.a.	75–90% P	struvite	0.5–3.5		Several	[49,85,89,90]
Struvite	domestic, anaerobic	6.5–10	n.a.	25–35	0.94	struvite	0.4		Shimamura et al., 2007	[91]
Struvite	domestic, anaerobic	n.a.	n.a.	1 m ³ /h	95% P	n.a.	0.56		Meng et al., 2021	[106]
Struvite	source-separated human urine	10	1.0	21 L (7)	95% P	struvite	1.5–3.5	(7)	Zamora et al., 2017	[87]
Struvite	activated carbon industry	29–96	0.9–1.5	5000 L (7)	50–90% P	struvite	0.5	(7)	Ye et al., 2021	[88]
Struvite	swine	2.4–4.8	1.5–4.5	100 L (7)	>95% P	struvite	2.5	(7)	Ye et al., 2016	[86]
Struvite	swine		1–5 h (1)	35	0.91	seedless	0.07	(1)(2)	Shim et al., 2020	[97]

¹Notes: n.a. not available, (1) hydraulic retention time, (2) circulating FBR, (3) FBR integrated with membrane operation, (4) aerated FBR, (5) synthetic wastewater, (6) influent flow rate, (7) reactor volume.

3.6. Metal Carbonates, Hydroxides, and Oxides

Application of FBRs for metals removal at full-scale has been realized since the 1980s to treat wastewaters from the metal plating, chlor-alkali, and other industries [6,7]. Relevant target metals were Cu, Ni, Co, Zn, among others. Metal precipitation as a carbonate is convenient because high recoveries are attainable, the metal may be readily recovered by acidification of the grains, and carbonate has a positive buffering effect on the treated water [6]. Recirculation is required for high influent concentrations. If the wastewater contains suspended solids, filtration upstream of the FBR is needed; otherwise, such solids act as seeds that promote formation of fine particles that are not retained in the FBR bed [6]. A list of the studies on metal removal with a FBR and some key processes and equipment parameters are given in Table 6.

Lewis [19,132] has found that both molecular growth and aggregation contribute to recovery from measurements of fines concentration along the bed height for the aqueous nickel hydroxy-carbonate system. She has also found that it is possible to favor growth by increasing the number of feed points and the effluent circulation rate, thereby increasing the recovery from 60 to 95%. For copper sulfide, the supersaturation was much higher, so this strategy was not effective, and recoveries were about 10% [19]. She has also found that low supersaturation results in decreased particle roughness, which reduces fines generation by abrasion of the grains. Lee et. al. [133] have studied the formation of copper carbonate in a FBR. They have found that particles formed by primary nucleation in solution aggregate to the seeds, forming a deposit that is porous and prone to abrasion. They have proposed to use low superficial velocities to reduce turbulence in the bed and to increase the specific surface of the grains. They have found that primary nucleation could be reduced by effective mixing of reactants at the bottom. A recovery of 96% was achieved. Lertratwattana et al. [134] have recovered copper from wastewater as the hydroxycarbonate of copper, malachite. The homogeneous FBR operated in two conditions to increase recovery: in the first 6 days a pH of 6.5 provided a low supersaturation suitable for initial development of the seeds, followed by a pH of eight. Lv et al. [131] have used a two-stage FBR to attain 96% recovery on a quartz seeded FBR. Wei et al. [135] have investigated CuCO_3 precipitation in a bench scale seeded FBR for 174 days. The removal efficiency was stable at 95%, but when the inlet supersaturation was allowed to increase, the efficiency decreased to 60–80% due to the generation of fines by primary nucleation in solution and seeds breaking. Adjusting of process conditions brought the system to the previous performance, showing the long-term feasibility of copper recovery. Copper and phosphate present in a wastewater from the semiconductor industry were removed as the basic phosphate $\text{Cu}_2\text{PO}_4\text{OH}$ by increasing the solution pH to 6 in a homogeneous FBR [136].

Nickel hydroxy carbonate with chemical formula $\text{Ni}(\text{OH})\text{CO}_3$ has been formed in FBRs at a pH of 9.7 via primary nucleation in solution followed by aggregation with seeds as well as by crystal growth upon the seeds. Reducing local supersaturation with multiple reactant feed points has increased recovery up to 99% [19,132]. At a higher pH value of 10.7 nullaginite, $\text{Ni}_2(\text{OH})_2\text{CO}_3$ has also led to a high recovery in a homogeneous FBR [137].

Lead recoveries of 99% have been found attainable as the carbonate salt at pH values of 8 to 10 and a carbonate-to-lead molar ratio of 3, using either heterogeneous seeds [138,139] or lead carbonate seeds with 0.057 mm in size prepared in a separate batch setup [140]. The same recovery has been found for a much less concentrated solution (0.19 mM) at the pH and carbonate-to-lead ratio just mentioned. Sand has been used as seed at a recycle ratio of 0.67.

A limited number of studies exist for other metals. Zinc has been precipitated as a mixture of hydrozincite, $\text{Zn}_5(\text{CO}_3)_2(\text{OH})_6$, and amorphous Zn compounds in a homogeneous FBR at a $\text{CO}_3:\text{Zn}$ molar ratio of 1.2 and a pH of 7.2 [141]. It has been found that ferric and chloride ions result in less crystalline solids and lower recoveries. The homogeneous FBR has yielded higher recoveries than FBRs seeded with hydrozincite and with silica sand. Wastewater from the aluminum industry has been treated with a homogeneous FBR to precipitate crystalline aluminum oxide with stoichiometry $\text{Al}_{2.66}\text{O}_4$ at pH 10.4 [142];

see details in Section 5 of this manuscript. Other metals removed with a FBR are silver carbonate [143] and titanium dioxide [144].

For wastewaters containing a mixture of heavy metals, effluent concentrations are slightly higher than in the case of a single metal [6]. Zhou et al. [145] have removed the metals Cu, Ni and Zn in a single FBR as the metal hydroxides at pH 9 with recovery of 95%. Lee et al. [146] have recovered the metals Cu, Pb, and Ni as carbonates and hydroxides. The pH value in the effluent of the FBR ranged from 8.7 to 9.1. Sequential FBRs have been used, with most of the metal ions being collected in the first reactor. Depending on solubilities and concentrations, it may be possible to selectively separate one or more metals [6].

3.7. Metal Sulfides

Metal sulfides precipitation in FBRs is deemed difficult because they involve extremely high supersaturations that promote the formation of colloidal, highly charged particles [18]. In spite of these difficulties, high recoveries of copper sulfide have been attained using a semicontinuous mode and calcium coated seeds [147]. In addition, arsenic trisulfide, As_2S_3 , has been removed with a high recovery after jar tests and experimental determination of the metastable zone width of the process [148]. Mixtures of cobalt and nickel sulfides were allowed to react with Na_2S in a FBR to yield recoveries of about 90% [149] without recirculation. Recoveries could be increased by using gaseous H_2S as reactant in a bubble FBR because slow gas dissolution has prevented local high supersaturation [149]. The process has been found suitable for wastewaters containing ~200 ppm metals but not for ~2,000 ppm.

3.8. Sulfate

Sulfate is commonly found in surface waters and in industrial waters, such as in ore beneficiation, paper mills, and fertilizer facilities. It forms scaling compounds that negatively interfere with water processing and with wastewater treatment with membrane operations. Sulfate also causes corrosion in sewers and negatively interferes with anaerobic wastewater treatment due to the action of sulfate reduction to sulfide by microbial action [150].

Sulfate removal in FBRs may be conducted with gypsum crystallization by reaction with added calcium chloride [151]. Recovery of gypsum in FBRs is probably controlled by crystal growth and abrasion of the grains [152]. Either alkaline or acid conditions may be chosen, which offers a good window to control coprecipitation of other impurities in the wastewater. For example, an influent solution containing sulfates of calcium, magnesium, and sodium with 1.1 mM total sulfate, has yielded grains containing both gypsum and magnesium hydroxide [153]. Ammonium or aluminum in solution favors a higher conversion [150]. Bare sand grains are not effective as a growth/aggregation substrate for gypsum, so in batch operation an initial period of low recovery may take place [154], while for continuous operation this material may be used. Another option is to use gypsum as seeds [151], as crystals of about 100 μm are easily developed in the FBR itself or in another crystallizer type. Seeding with silica or gypsum are equally effective for recovery [153]. For an influent concentration of 160 mM, optimal conditions are a Ca/SO_4 molar ratio of 1.48, a superficial velocity of $0.032 \text{ m} \cdot \text{min}^{-1}$ and a recirculation-to-feed ratio of 32, which yields a sulfate conversion of 82% and recovery of 67% [150]. Gypsum crystallization in FBRs is sometimes applied aiming at calcium removal [56].

3.9. Boron

Boron removal may be accomplished by adding hydrogen peroxide and a divalent metal to convert boric acid into a slightly soluble perborate salt. This chemistry has been applied to a homogeneous FBR to precipitate calcium perborate compounds [155]. Additionally, barium from another wastewater has been used as a reactant, having either silica sand or a waste-derived mesoporous aluminosilicate. The latter seed type was found superior due to its ability to adsorb barium ions on its surface, which promote heterogeneous nucleation of the target boron compound on its surface [156].

Table 6. Metals removal in FBR reactors.

Target Element	Inlet Concentration (mM)	Superficial Velocity (m/min)	Bed Diameter (cm)	Recovery (%)	Crystallizing Compound	Seed Material	Grain Size (mm)	Note	References
Al	12	0.25–0.6	2	97%	$Al_{2.66}O_4$	Seedless	0.25		[142]
Al	6.6	0.22	2	99%	$Al(OH)_3$ Bayerite	Seedless	0.5		[157]
As	500–1000 ppm	0.02	2	97%	As_2S_3 Arsenic trisulfide	Silica sand	-	Aerated FBR	[148]
B	185	0.42	3.5	60%	$CaB(OH)_3OOB(OH)_3$ and $Ca(B(OH_3)OOH)_2$ Amorphous calcium perborate	Seedless	1		[155]
B	200	0.05	2	93%	$BaB_2(OO)_2(OH)_4$ barium peroxoborate	Mesoporous aluminosilicate		Barium adsorbs on seed surface	[156]
Ba	-	0.48	-	98%	$BaHPO_4$ and BaO at pH < 10 $Ba_3(PO_4)_2$ at pH 11	Seedless	0.8–1.0	Seeding had no effect	[116]
Ca	10	0.2	2	90%	$CaCO_3$	Seedless	1–2		[73,158]
Cu	10 ppm	0.41	3	96%	$CuCO_3$	Quartz	-		[133]
Cu	6–8	0.032	2	92%	$Cu_2CO_3(OH)_2$ malachite	Seedless	<0.3	Dual pH	[134]
Cu	20–50 ppm	0.22	3	95%	Probably $Cu_2CO_3(OH)_2$	Quartz	0.3	174 days	[135]
Cu P	6.5	0.032	2	96%	Cu_2PO_4OH	Seedless	1		[136]
Ni	100 ppm	0.24	2.5	99%	$Ni(OH)CO_3$	Quartz	-		[132,159,160]
Ni	200	0.16	2	98%	$Ni_2(OH)_2CO_3$ Nullaginite	Seedless	0.15–0.5	granules visible in 4–5 days	[137]
Pb	0.19	0.37		99%	$PbCO_3$	sand			[138].
Pb	2.4	0.16	4	99%	Cerussite $PbCO_3$	garnet			[139]

Table 6. Cont.

Target Element	Inlet Concentration (mM)	Superficial Velocity (m/min)	Bed Diameter (cm)	Recovery (%)	Crystallizing Compound	Seed Material	Grain Size (mm)	Note	References
Pb	48	5.6	5.2	99%	PbCO ₃	PbCO ₃		Seeds prepared in a batch reactor	[140]
Zn	7.6	0.9–5.4	2	86–92%	Zn(CO ₃) ₂ (OH) ₆ Hydrozincite	Seedless	0.04–0.15	Cl ⁻ and Fe ³⁺ decrease granule size	[141]
Cu Ni Zn	10–20 ppm	0.31	1	95%	Mixture of metal carbonates with metal hydroxides	Quartz			[145]
Cu Pb Ni	130 to 250 ppm			93 to 98%	Mixture of metal carbonates and hydroxides			FBRs in series	[146]
Co, Cu	30	0.7	2	96%	Co ₃ (PO ₄) ₂ ·8H ₂ O and Cu ₂ (PO ₄)OH	Seedless	0.7		[118]
Ni Co					sulfides				[19,149]
F	0.5–250	0.07–0.6	2	98%	CaF ₂	Seedless	<0.2		[119]
Oxalate	150–450			95%	CaC ₂ O ₄ ·H ₂ O	Seedless	0.15		[161]
Oxalate	3	0.1	2	82%	CaC ₂ O ₄ ·H ₂ O	Seedless	0.3–1.0		[162]
P	16	0.06	2	90%	CaHPO ₄ ·2H ₂ O brushite	Seedless	0.5		[163]
P	100	-	-	86%	Mg ₂ PO ₄ OH and Mg ₃ (PO ₄) ₂	Seedless	<1	Recovery with seeds was 93%	[111]
S	80–160		5.2	66%	Gypsum CaSO ₄ ·2H ₂ O	Sand, gypsum			[150,151]

4. Integration with Other Unit Operations

4.1. FBR and Membrane Operations

Membrane operations, such as reverse osmosis and electrodialysis, are applied for water reuse within industry and as part of wastewater treatment. The water recovery is often limited by scaling of slightly soluble contaminants upon the membrane surfaces. Consequently, removing scaling components upstream of the membrane operation or between membrane stages leads to improved water recoveries. Precipitation techniques are so far the only options developed to a full-scale, the FBR has the advantages of a reduced footprint, chemical demand, and sludge generation, in spite of a higher capital cost [164]. The combination of FBRs with membranes has been applied for the treatment of wastewater [165], brackish groundwater [55,56,127,164,166], and drinking water [167,168]. Usually, the target compound is calcium carbonate [70,128,167,169,170], but other compounds may also be separated, such as calcium sulfate dihydrate [56], a mixture of calcium carbonate and nickel hydroxide [171], a mixture of calcium carbonate and magnesium compounds [165], as well as calcium phosphate [172].

Membranes have also been used to improve the performance of the FBR. In analogy with the membrane assisted suspension crystallizer originally proposed by Sluys et al. [173], Li and collaborators [128] have immersed an ultrafiltration membrane in the fluidized bed, so only the solution leaves the crystallizer.

Nanofiltration of seawater has been used to produce a low-cost magnesium solution, as this element is present at high concentrations in the oceans (~1400 mg/L) and is efficiently rejected by nanofiltration membranes. The solution has been fed to a FBR to crystallize struvite, $\text{NH}_4\text{MgPO}_4 \cdot 6\text{H}_2\text{O}$, reducing the cost of the process for treating the supernatant of a domestic-sludge dewatering facility [107]. As seawater contains other impurities for which nanofiltration rejection is variable, FBR pH and magnesium dosage had to be adjusted to avoid both undesirable calcium phosphate precipitation, and sodium and chloride excessive wastewater salinity. For a nanofiltration rejection of 90%, more than 90% of P removal was achieved, and the struvite purity was ~95%. Struvite precipitation was conducted in the presence of an antifouling agent, which was added to the NF brine to prevent the clogging of the NF membrane.

4.2. FBR and Adsorption

FBR and adsorption are combined by using an adsorber as seeds in the FBR. The method allows faster adsorption than in a fixed bed and potentially uses a waste as an adsorbate. The disadvantage is that the adsorbed compound is not recovered in concentrated form. Lee et al. [174] have seeded a FBR with the sludge from a water clarifier. Over 90% of the copper in the wastewater was removed by simultaneous adsorption and precipitation of copper hydroxide upon the sludge particles. During removal from organic compounds by Fenton oxidation and adsorption, simultaneous precipitation of Fe(III) hydroxides upon the seeds substantially reduced downstream sludge formation [175–178].

4.3. FBR and Absorption for Carbon Capture from Air

A proprietary process has been proposed [179] in which CO_2 is absorbed from air with a KOH solution to form a K_2CO_3 solution; see Figure 6. This solution is treated with $\text{Ca}(\text{OH})_2$ in a FBR to separate CO_3 as CaCO_3 and to recover the KOH solution. The FBR yields the calcium carbonate as large particles that upon calcination are converted into the desired concentrated CO_2 suitable for further processing or storage and a solid CaO stream. This oxide then converted into $\text{Ca}(\text{OH})_2$ that returns to the FBR. The FBR differs from those used in water softening because the carbonate concentration is much larger, ~0.5 against ~0.005 M, and the pH is higher. It has been found that for pH values in the range of 12 to 14 vaterite is formed, whereas for lower values calcite is the dominant polymorph, but carbonate recovery is not significantly affected by the pH [180].

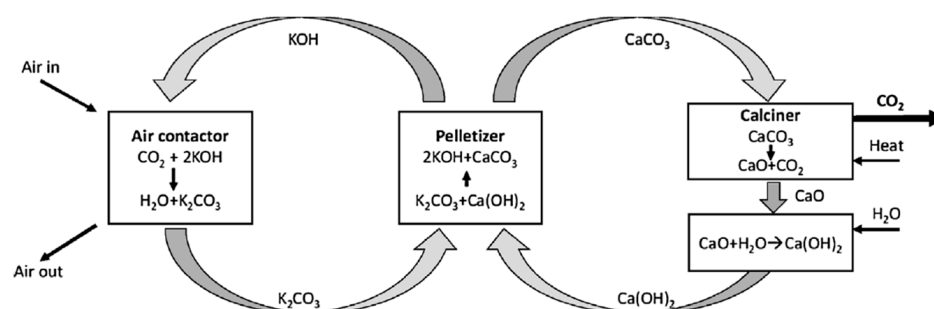


Figure 6. Process for carbon capture from air involving a FBR. Source [179].

4.4. FBR and Biological Process for Treatment of Acid Mine Drainage

Wastewater derived from mining operations are typically acidic and contain sulfate and metals that must be removed before discharge to surface waters. Sulfate reducing bacteria may produce hydrogen sulfide that subsequently reacts with metals to form metal sulfide precipitates. The reader is referred to nice reviews on this topic [181,182], here just a brief description is given. Biological sulfate reduction and chemical reaction crystallization may be simultaneously conducted in a fluidized bed bioreactor. This configuration has advantages in relation to other bioreactors because it offers a large surface area for microorganism growth, high mass transfer rate, among others. Much like in a conventional FBR, the metal sulfide precipitate may be found on the surface of the (biofilm) seeds, in the effluent as fine particles or in solution. The concentration in solution is usually very low because of the low metal sulfides solubilities. When an inverted fluidized bed design is used, the precipitates may be collected separately from the biomass. The inverted bed is designed with biofilm carriers of low density, so the influent flows downward, with the biomass being collected at the top and the metal precipitate at the bottom. It is also possible to precipitate the metals in a separate reactor, for instance, upstream from the biological FBR by recirculation of the effluent containing sulfide or H_2S . Metal sulfides precipitation is advantageous in comparison to conventional metal hydroxide precipitation because the required hydraulic retention times are lower, the effluent concentration is an order of magnitude lower, and the sludge is more compact and easier to dewater.

5. Improved FBR Concepts

5.1. Aerated FBR

Segev et al. [127] have proposed to crystallize calcium carbonate in a FBR by simply inserting an air stream into the fluidized bed. This is an improvement in relation to the well-developed softening operation which promotes crystallization with the aid of a chemical, usually calcium hydroxide. Calcium carbonate precipitation relies on the pH increase promoted by the release of part of the carbonate originally in solution as CO_2 to the air stream. This route is feasible only for solutions with a high carbonate content. The authors propose to apply the process in desalination of brackish waters for production of drinking water and to aid reverse osmosis operation by removing scale-forming calcium carbonate. A mathematical model for the process has been developed that is useful for design [61]. CO_2 stripping with air has also been used for pilot-scale decarbonation of geothermal waters [129], to keep a high pH during struvite crystallization in a FBR [110], for phosphate removal from dairy and swine wastewater as struvite or mixtures of struvite and calcium carbonate [100], and as a means of improving fluid dynamics during recovery in copper removal from metal industry wastewater [131].

5.2. Circulating FBR

Hu et al. [9] have introduced an annular zone within the cylindrical fluidized bed to promote circulation of the grains; see Figure 7. Consequently, the particle size does not vary with bed height. The authors conclude that this configuration requires a reduced bed height and allows for an improved recovery and an extended discharge time of grains.

Experimental data for two industrial scale units have been presented [8,9]. Another modification of the bed, including three concentric sections, has been applied for simultaneous removal of calcium, magnesium, and silica [130] by dosing precipitation agents (NaOH and MgO) and flocculants (aluminum sulfate and polyacrylamide). Circulation of the grains within the bed is also promoted by adding one of the reactants through a nozzle in the upward direction [97]. The upper part of the bed may have a conical shape to provide a settling zone, so only the smallest particles leave the system in the overflow. Recirculation of the FBR effluent has also been applied to retain part of the fine particles in the bed [97].

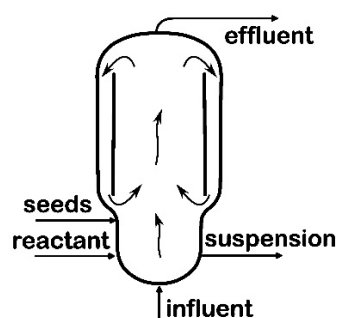


Figure 7. Circulating fluidized bed introduced by Hu et al. [9].

5.3. Homogeneous FBR

The basic idea of a classic FBR is to allow compounds that would otherwise develop as micrometer-sized particles to attach to large seed particles of a suitable support material. However, for some systems it has been shown that, even in the absence of seeds, it is possible to develop submillimeter- or millimeter-sized particles of the target compound in the FBR. During the startup period, which may last a few hours to a few days, a low superficial velocity and a high recirculation ratio of the suspension leaving the reactor may be required. Glass beads of a few centimeters in diameter are often added at the bottom at the point of the reactants addition to prevent clogging and formation of bubbles [157]. Once a fluid bed develops, operation is like a seeded FBR, with the advantage that the particles are constituted by the pure target compound. This type of crystallizer is known as homogeneous granulation FBR. Applications of homogeneous FBRs described in Table 6 encompass crystallization of fifteen compounds and their mixtures. Recoveries are generally above 90% and grains sizes range from 0.1 to 1 mm, thus similar to classic FBRs. The superficial velocities are highly variable; in general, they lie within the range of 0.05 to 0.5 $\text{m}\cdot\text{min}^{-1}$. So far, the processes have been developed to the bench scale. Aluminum removal as bayerite (aluminum hydroxide) was conducted at a pH of 9.2 and a molar ratio of $\text{H}_2\text{O}_2/\text{Al}$ of 2 [157]. A low superficial velocity 0.22 $\text{m}\cdot\text{min}^{-1}$ was used at the start to allow for growth of the fluidized particles, which were retained in an upper section of the bed with a diameter twice the main crystallizer body. Later, a superficial velocity of 0.5 $\text{m}\cdot\text{min}^{-1}$ and a recirculation-to-feed ratio of three were used. In another application, aluminum oxide with stoichiometry $\text{Al}_{2.66}\text{O}_4$ developed as 0.25 mm sized granules, but a startup period of 11 days was required [142]. Calcium fluoride has also been removed with large recovery even for high influent concentrations of 10,000 ppm F^- [119]. A calcium carbonate recovery of 90% and compact granules of 1 to 2 mm have been obtained, with the pH being the most important variable not only for recovery but also for particle size, shape, and crystallinity [73,158]. Zinc wastewater from the mechanical industry wastewater was treated to yield a recovery of about 90%, but chloride and ferric ions reduced the recovery and the granule size and were incorporated in the particles [141]. Thin-film transistors liquid crystal display industry produces a phosphate-rich effluent, which yielded magnesium phosphate as a mixture of salts [111]. Barium removal with phosphates yielded different solid compounds depending on the pH. Homogeneous and seeded processes resulted in the same high recovery of 98% [116].

5.4. Separation of Enantiomers

Cooling crystallization is commonly applied for the separation of enantiomers from racemic mixtures. Crystallization of the desired enantiomer is promoted by seeding with the same material in a mixed suspension. Batch operation is usually applied for flexibility, but continuous configuration is potentially more economical and meets more stringent product quality demands. A continuous selective crystallization process has been proposed [183,184] that consists of two crystallizers, one for each enantiomer. The liquid recirculates among the two crystallizers, so its composition does not change much while allowing for a substantial yield. The FBR has been proposed as an alternative crystallizer [62] with some advantages. A slightly conical geometry enhances particle segregation by size, enabling extraction of the product of desired particle size in a conveniently located outlet port. Additionally, small particles that formed in solution, possibly of the undesired enantiomer, are readily removed with the upflowing liquid and redissolved in the feed tank. Further, particles larger than the product are removed from the bottom, crushed, and reinserted in the FBR as seeds, exempting the need for a dedicated unit for seeds' preparation. The process has also proven to offer higher yield (in mass of product per hour per volume crystallizer) than a batch process for the enantiomers of asparagine monohydrate [63,185]. CFD-DEM modeling has been applied to improve reactor geometry [43,186]. Besides enantiomers, also other stereoisomers (positional isomers OABA and PABA) could be continuously separated in FBRs [187].

5.5. FBR with Supercritical Fluids

Supercritical CO₂ has found increased use as an antisolvent for the production of micro- and nanoparticles in the pharmaceutical and food applications [188]. In the so-called RESS process (rapid expansion of supercritical solutions), the target compound is initially dissolved in supercritical CO₂ and precipitates as the fluid expands upon flowing through a nozzle. In the SAS process (supercritical antisolvent), the target compound is initially in a solution with a solvent and precipitates upon mixing with supercritical CO₂. The nanoparticles are not used as such, instead microencapsulated or nanoencapsulated particles are required to provide desirable bioavailability or surface properties [188]. Production of such capsules in FBRs combined with the RESS and SAS processes received attention in recent years. Fluidization with supercritical CO₂ has been found to obey well known correlations for fluidization [189]. The FBR-RESS process proposed in 1985 [190] consists of a circulating fluidized bed with an internal nozzle at the center of the riser, which provides rapid expansion of a supercritical fluid solution. The fluid in expansion provides fluidization of seeds and promotes precipitation of the target compound upon the seeds. The method has been applied for five compounds that mimic actual active pharmaceuticals on microcrystalline cellulose seeds, which is a well-known excipient, suggesting that the method may be applied to many active compounds [191]. In the FBR-SAS process, the supercritical CO₂ is added at the bottom of the fluidized bed through a sintered plate distributor to provide fluidization of excipient particles. A solution of the active compound is added at the bottom, where it mixes with CO₂ and precipitates upon the excipient particles [192]. The method has been applied to the deposition of the active compound narigin on the excipient microcrystalline cellulose [192], curcumin on lactose [193], curcumin and poly (vinyl pyrrolidone) on microcrystalline cellulose (MCC, 175 µm), corn starch (15 µm) and lactose (<5 µm) [194], and sirolimus on microcrystalline cellulose, lactose, and sucrose [195]. It has been suggested that the approach could be transferred to other industries where release is important, such as agrochemical, cosmetic, and food [192].

6. Conclusions

In fluidized bed reactors, the undesirable processing features of micrometer-sized particles are circumvented by the use of large, millimeter-sized seeds. The resulting large particles may be easily separated from the solution and used as a valuable product. Liquid residence times of only a few minutes are commonly found, so the process is suitable for

treatment of large streams. Full-scale applications for softening of drinking water are in use since the 1980s. Since then, full-scale units were implemented for phosphate removal from wastewaters as struvite and calcium phosphate, as well as for metal removal from wastewater. Full-scale experiences exist with the improved design of the circulating FBR for softening of industrial water and drinking water. Additionally, new applications have been developed or are in development for recovery of fluoride, sulfate, boron, among others.

Process integration with other unit operations have been proposed to address a number sustainability demands, as shown in the following examples. In desalination and in water treatment for reuse with zero liquid discharge, metals precipitation in the FBR are combined with membrane processes to reduce scaling upon membrane surfaces, thereby reducing energy demand. FBRs seeded with an adsorbent offer perspective of improved recovery and use of waste materials as seeds. Aiming at carbon capture from air, calcium carbonate precipitation in FBRs is combined with absorption and calcination operations to form an efficient closed system. In the treatment of acid mine drainage, metals sulfide precipitation in FBRs are integrated with biogenically produced H_2S and HCO_3 with low energy and chemicals demand.

Recently, novel FBR concepts have been proposed: the aerated FBR allows chemical-free precipitation of calcium carbonate for wastewaters containing high carbonate content; a seedless FBR, known as the homogeneous granulation FBR, yields a pure particulate product; the circulating FBR offers economic recovery of the target compound and extended utilization of the seeds; coupled FBRs have been developed for separation of chiral compounds; FBRs with supercritical fluids precipitate core-shell particles suitable as pharmaceutical formulations.

Fundamental studies have elucidated the elementary steps of crystallization in FBRs. Crystal growth is the dominant process for the formation of calcium carbonate, whereas agglomeration is important for calcium phosphate, metal sulfides and struvite particles. Grains in a FBR have varying density and size, so they tend to segregate to minimize the potential energy, but they also mix due to turbulence. These phenomena have been incorporated in population, mass, and energy balances to describe certain experimental systems. Consequently, mathematical models have been extensively used for process improvement, optimization, and control of bench, pilot, and full-scale units.

7. Future Perspectives

Crystallization of a few compounds in FBRs is well established, but many opportunities exist to expand the list of crystallization systems to be applied at full-scale. To this end, many existing nice studies linking fundamentals and mathematical models with pilot-scale experiments might serve as inspiration to support the development of robust processes with sufficient maturity for scaleup.

There is room for the development of new applications of FBRs by integration with other unit operations such as membrane, adsorption, and absorption. In such cases, knowledge of FBR behavior for existing compounds will have to be extended to new conditions. When precipitation occurs simultaneously to adsorption and microorganisms' growth, little attention has so far been paid to the precipitation aspects of the process.

Recent promising developments such as the aerated FBR and the homogeneous granulation FBR have so far been developed to the bench scale, more research on a larger scale and on the fundamentals of these processes are needed. The circulating FBR has already been applied in full-scale for calcium carbonate precipitation, extension for other systems would be welcome.

The fluidization behavior of calcium carbonate seeded systems has been thoroughly studied. For other systems, more research is needed on the morphology, shape, and mechanical properties of the particles. The residence time of solids is in the order of days or even months, so long duration experiments are needed.

FBR mathematical models usually consider simple precipitation kinetics fitted to experiments with lumped parameters. A better knowledge is needed on the true kinetics of

crystal growth, agglomeration, and abrasion. The roles of primary nucleation in solution, crystal growth upon the grains, and grains' abrasion on FBR performance is not always well understood. Additionally, many FBR processes include recirculation of the effluent, so fine particles are introduced in the reactor, contributing to recovery in poorly understood ways. "Single pass" performance indicators for FBRs, which would be useful for both process understanding and design, are scarce. Studies considering the true supersaturation along the bed height and about the metastable zone width would help elucidate the true kinetics in FBRs.

Funding: The author gratefully acknowledges the financial support of the RCGI—Research Centre for Greenhouse Gas Innovation, hosted by the University of São Paulo (USP) and sponsored by FAPESP—São Paulo Research Foundation (2014/50279-4 and 2020/15230-5 Project 66 GHG-3) and Shell Brazil, and the strategic importance of the support given by ANP (Brazil's National Oil, Natural Gas and Biofuels Agency) through the R&D levy regulation. The author also acknowledges the funding of FAPESP, Process numbers n° 20/15230-5, 17/19087-0, 14/14289-5.

Conflicts of Interest: The authors declare no conflict of interest.

References

1. Lewis, A.E.; Seckler, M.M.; Kramer, H.; Van Rosmalen, G.M. *Industrial Crystallization: Fundamentals and Applications*; Cambridge University Press: Cambridge, UK, 2015; ISBN 9781107280427.
2. Gledhill, E.G.; McCanlis, A.W.H. Softening of chalk well water and river water in a pellet reactor followed by upward flow sand filtration. *Water Treat. Exam* **1970**, *19*, 51–69.
3. Hilson, M.A.; Law, F. Softening of bunter sandstone waters and river waters of varying qualities in pellet reactors. *Water Treat. Exam* **1970**, *19*, 32–50.
4. Van Dijk, J.C.; Braakensiek, H. Phosphate Removal by Crystallization in a Fluidized Bed. *Water Sci. Technol.* **1985**, *17*, 133–142. [[CrossRef](#)]
5. Seckler, M.M.; Bruinsma, O.S.L.; Van Rosmalen, G.M.; Van Dijk, J.C.; Delgorge, F.; Eggers, J. Phosphate removal by means of a full scale pellet reactor. In Proceedings of the 11th Symposium Industrial Crystallization, Garmisch-Partenkirchen, Germany, 18–20 September 1990.
6. Schöller, M.; van Dijk, J.C.; van Haute, A.; Wilms, D.; Pawłowski, L.; Wasag, H. Recovery of Heavy Metals by Crystallization in the Pellet Reactor, a Promising Development. *Stud. Environ. Sci.* **1988**, *34*, 77–90. [[CrossRef](#)]
7. Scholler, M.; van Dijk, J.C.; Wilms, D. Recovery of heavy metals by crystallization. *Met. Finish.* **1987**, *85*, 31–34.
8. Hu, R.; Huang, T.; Wang, T.; Wang, H.; Long, X. Application of Chemical Crystallization Circulating Pellet Fluidized Beds for Softening and Saving Circulating Water in Thermal Power Plants. *Int. J. Environ. Res. Public Health* **2019**, *16*, 4576. [[CrossRef](#)]
9. Hu, R.; Huang, T.; Zhi, A.; Tang, Z. Full-scale experimental study of groundwater softening in a circulating pellet fluidized reactor. *Int. J. Environ. Res. Public Health* **2018**, *15*, 1592. [[CrossRef](#)]
10. Van Ammers, M.; Van Dijk, J.C.; Graveland, A.; Nuhn, P.A.N.M. State of the art of pellet softening in the Netherlands. *Water Supply* **1986**, *4*, 223–235.
11. Harms, W.D.; Robinson, R.B. Softening by fluidized bed crystallizers. *J. Environ. Eng.* **1992**, *118*, 513–529. [[CrossRef](#)]
12. Liu, Y.; Kumar, S.; Kwag, J.-H.; Ra, C. Magnesium ammonium phosphate formation, recovery and its application as valuable resources: A review. *J. Chem. Technol. Biotechnol.* **2013**, *88*, 181–189. [[CrossRef](#)]
13. Le Corre, K.S.; Valsami-Jones, E.; Hobbs, P.; Parsons, S.A. Phosphorus Recovery from Wastewater by Struvite Crystallization: A Review. *Crit. Rev. Environ. Sci. Technol.* **2009**, *39*, 433–477. [[CrossRef](#)]
14. Gui, L.; Yang, H.; Huang, H.; Hu, C.; Feng, Y.; Wang, X. Liquid solid fluidized bed crystallization granulation technology: Development, applications, properties, and prospects. *J. Water Process Eng.* **2022**, *45*, 102513. [[CrossRef](#)]
15. Hu, R.; Huang, T.; Wen, G.; Yang, S. Modelling particle growth of calcium carbonate in a pilot-scale pellet fluidized bed reactor. *Water Supply* **2017**, *17*, 643–651. [[CrossRef](#)]
16. Rankin, A.H.; Sutcliffe, P.J.C. Morphology, chemistry and growth mechanisms of calcite concretions from an industrial water-softening process: Implications for the origin of natural ooids in sediments. *Proc. Geol. Assoc.* **1999**, *110*, 33–40. [[CrossRef](#)]
17. Seckler, M.M. Calcium Phosphate Precipitation in a Fluidized Bed. Ph.D. Thesis, Delft University of Technology, Delft, The Netherlands, 1994.
18. Mokone, T.P.; van Hille, R.P.; Lewis, A.E. Metal sulphides from wastewater: Assessing the impact of supersaturation control strategies. *Water Res.* **2012**, *46*, 2088–2100. [[CrossRef](#)] [[PubMed](#)]
19. Lewis, A.E. Fines Formation (and Prevention) in Seeded Precipitation Processes. *KONA Powder Part. J.* **2006**, *24*, 119–125. [[CrossRef](#)]
20. Bhuiyan, M.I.H.; Mavinic, D.S.; Beckie, R.D. Nucleation and growth kinetics of struvite in a fluidized bed reactor. *J. Cryst. Growth* **2008**, *310*, 1187–1194. [[CrossRef](#)]

21. Fromberg, M.; Pawlik, M.; Mavinic, D.S. Induction time and zeta potential study of nucleating and growing struvite crystals for phosphorus recovery improvements within fluidized bed reactors. *Powder Technol.* **2020**, *360*, 715–730. [[CrossRef](#)]
22. Zeng, G.; Ling, B.; Li, Z.; Luo, S.; Sui, X.; Guan, Q. Fluorine removal and calcium fluoride recovery from rare-earth smelting wastewater using fluidized bed crystallization process. *J. Hazard. Mater.* **2019**, *373*, 313–320. [[CrossRef](#)]
23. Seckler, M.M.; Bruinsma, O.S.L.; Van Rosmalen, G.M. Phosphate removal in a fluidized bed—I. Identification of physical processes. *Water Res.* **1996**, *30*, 1585–1588. [[CrossRef](#)]
24. Seckler, M.M.; Bruinsma, O.S.L.; Van Rosmalen, G.M. Calcium phosphate precipitation in a fluidized bed in relation to process conditions: A black box approach. *Water Res.* **1996**, *30*, 1677–1685. [[CrossRef](#)]
25. Montastruc, L.; Azzaro-Pantel, C.; Biscans, B.; Cabassud, M.; Domenech, S. A thermochemical approach for calcium phosphate precipitation modeling in a pellet reactor. *Chem. Eng. J.* **2003**, *94*, 41–50. [[CrossRef](#)]
26. Iqbal, M.; Bhuiyan, M.I.H.; Mavinic, D.S. Assessing struvite precipitation in a pilot-scale fluidized bed crystallizer. *Environ. Technol.* **2008**, *29*, 1157–1167. [[CrossRef](#)] [[PubMed](#)]
27. Xu, K.; Ge, L.; Wang, C. Effect of upflow velocity on the performance of a fluidized bed reactor to remove phosphate from simulated swine wastewater. *Int. Biodeterior. Biodegrad.* **2019**, *140*, 78–83. [[CrossRef](#)]
28. Tai, C.Y.; Chien, W.-C.; Chen, C.-Y. Crystal growth kinetics of calcite in a dense fluidized-bed crystallizer. *AIChE J.* **1999**, *45*, 1605–1614. [[CrossRef](#)]
29. Tai, C.Y. Crystal growth kinetics of two-step growth process in liquid fluidized-bed crystallizers. *J. Cryst. Growth* **1999**, *206*, 109–118. [[CrossRef](#)]
30. Aldaco, R.; Garea, A.; Irabien, A. Modeling of particle growth: Application to water treatment in a fluidized bed reactor. *Chem. Eng. J.* **2007**, *134*, 66–71. [[CrossRef](#)]
31. Aldaco, R.; Garea, A.; Irabien, A. Particle growth kinetics of calcium fluoride in a fluidized bed reactor. *Chem. Eng. Sci.* **2007**, *62*, 2958–2966. [[CrossRef](#)]
32. Seckler, M.M.; Bruinsma, O.S.L.; Van Rosmalen, G.M. Influence of Hydrodynamics on Precipitation: A Computational Study. *Chem. Eng. Commun.* **1995**, *135*, 113–131. [[CrossRef](#)]
33. Richardson, J.F.; Backhurst, J.R.; Harker, J.H. Coulson & Richardson's Chemical engineering. In *Particle Technology and Separation Processes*; Butterworth Heinemann: Oxford, UK, 2002; Volume 2.
34. Kramer, O.J.I.; de Moel, P.J.; Padding, J.T.; Baars, E.T.; El Hasadi, Y.M.F.; Boek, E.S.; van der Hoek, J.P. Accurate voidage prediction in fluidisation systems for full-scale drinking water pellet softening reactors using data driven models. *J. Water Process Eng.* **2020**, *37*, 101481. [[CrossRef](#)]
35. Ye, X.; Chu, D.; Lou, Y.; Ye, Z.-L.; Wang, M.K.; Chen, S. Numerical simulation of flow hydrodynamics of struvite pellets in a liquid–solid fluidized bed. *J. Environ. Sci.* **2017**, *57*, 391–401. [[CrossRef](#)] [[PubMed](#)]
36. Toyokura, K.; Tanaka, H.; Tanahashi, J. Size Distribution of Crystals from Classified Bed Type Crystallizer. *J. Chem. Eng. Jpn.* **1973**, *6*, 325–331. [[CrossRef](#)]
37. Frances, C.; Biscans, B.; Laguerie, C. Modelling of a continuous fluidized-bed crystallizer effects of mixing and segregation on crystal size distribution during the crystallization of tetrahydrate sodium perborate. *Chem. Eng. Sci.* **1994**, *49*, 3269–3276. [[CrossRef](#)]
38. Shiao, L.-D.; Lu, T.-S. Interactive Effects of Particle Mixing and Segregation on the Performance Characteristics of a Fluidized Bed Crystallizer. *Ind. Eng. Chem. Res.* **2001**, *40*, 707–713. [[CrossRef](#)]
39. Al-Rashed, M.; Wójcik, J.; Plewik, R.; Synowiec, P.; Kuś, A. Multiphase CFD modeling-scale-up of Fluidized-Bed Crystallizer. *Comput. Aided Chem. Eng.* **2009**, *26*, 695–700. [[CrossRef](#)]
40. Al-Rashed, M.; Wójcik, J.; Plewik, R.; Synowiec, P.; Kuś, A. Multiphase CFD modeling: Fluid dynamics aspects in scale-up of a fluidized-bed crystallizer. *Chem. Eng. Process. Process Intensif.* **2013**, *63*, 7–15. [[CrossRef](#)]
41. Rahaman, M.S.; Choudhury, M.R.; Ramamurthy, A.S.; Mavinic, D.S.; Ellis, N.; Taghipour, F. CFD modeling of liquid-solid fluidized beds of polydisperse struvite crystals. *Int. J. Multiph. Flow* **2018**, *99*, 48–61. [[CrossRef](#)]
42. van Schagen, K.M.; Rietveld, L.C.; Babuška, R.; Kramer, O.J.I. Model-based operational constraints for fluidised bed crystallisation. *Water Res.* **2008**, *42*, 327–337. [[CrossRef](#)]
43. Kerst, K.; Roloff, C.; Medeiros de Souza, L.G.; Bartz, A.; Seidel-Morgenstern, A.; Thévenin, D.; Janiga, G. CFD-DEM simulations of a fluidized bed crystallizer. *Chem. Eng. Sci.* **2017**, *165*, 1–13. [[CrossRef](#)]
44. Kennedy, S.C.; Bretton, R.H. Axial dispersion of spheres fluidized with liquids. *AIChE J.* **1966**, *12*, 24–30. [[CrossRef](#)]
45. Patwardhan, V.S.; Tien, C. Distribution of solid particles in liquid fluidized beds. *Can. J. Chem. Eng.* **1984**, *62*, 46–54. [[CrossRef](#)]
46. Dutta, B.K.; Bhattacharya, S.; Chaudhury, S.; Barman, B. Mixing and segregation in a liquid fluidized bed of particles with different size and density. *Can. J. Chem. Eng.* **1988**, *66*, 676–680. [[CrossRef](#)]
47. Gibilaro, L.G.; Di Felice, R.; Waldram, S.P.; Foscolo, P.U. A predictive model for the equilibrium composition and inversion of binary-solid liquid fluidized beds. *Chem. Eng. Sci.* **1986**, *41*, 379–387. [[CrossRef](#)]
48. Van Schagen, K.M.; Rietveld, L.C.; Babuška, R. Dynamic modelling for optimisation of pellet softening. *J. Water Supply Res. Technol.* **2008**, *57*, 45–56. [[CrossRef](#)]
49. Rahaman, M.S.; Mavinic, D.S.; Meikleham, A.; Ellis, N. Modeling phosphorus removal and recovery from anaerobic digester supernatant through struvite crystallization in a fluidized bed reactor. *Water Res.* **2014**, *51*, 1–10. [[CrossRef](#)]

50. Rahaman, M.S.; Mavinic, D.S.; Ellis, N. Phosphorus recovery from anaerobic digester supernatant by struvite crystallization: Model-based evaluation of a fluidized bed reactor. *Water Sci. Technol.* **2008**, *58*, 1321–1327. [[CrossRef](#)]
51. Wang, J.; Ye, X.; Zhang, Z.; Ye, Z.-L.; Chen, S. Selection of cost-effective magnesium sources for fluidized struvite crystallization. *J. Environ. Sci.* **2018**, *70*, 144–153. [[CrossRef](#)]
52. Zhang, C.; Xu, K.; Li, J.; Wang, C.; Zheng, M. Recovery of Phosphorus and Potassium from Source-Separated Urine Using a Fluidized Bed Reactor: Optimization Operation and Mechanism Modeling. *Ind. Eng. Chem. Res.* **2017**, *56*, 3033–3039. [[CrossRef](#)]
53. Montastruc, L.; Azzaro-Pantel, C.; Biscans, B.; Cabassud, M.; Domenech, S.; Dibouveau, L. A General Framework for Pellet Reactor Modelling: Application to P-Recovery. *Chem. Eng. Res. Des.* **2003**, *81*, 1271–1278. [[CrossRef](#)]
54. Montastruc, L.; Azzaro-Pantel, C.; Pibouleau, L.; Domenech, S. A systemic approach for pellet reactor modeling: Application to water treatment. *AIChE J.* **2004**, *50*, 2514–2525. [[CrossRef](#)]
55. Choi, J.Y.; Kaufmann, F.; Rahardianto, A.; Cohen, Y. Corrigendum to ‘Desupersaturation of RO concentrate and gypsum removal via seeded precipitation in a fluidized bed crystallizer’ [Water Research 190 (2021)]. *Water Res.* **2021**, *193*, 116943. [[CrossRef](#)] [[PubMed](#)]
56. Choi, J.Y.; Kaufmann, F.; Rahardianto, A.; Cohen, Y. Desupersaturation of RO concentrate and gypsum removal via seeded precipitation in a fluidized bed crystallizer. *Water Res.* **2021**, *190*, 116766. [[CrossRef](#)] [[PubMed](#)]
57. van Schagen, K.M.; Babuška, R.; Rietveld, L.C.; Baars, E.T. Optimal flow distribution over multiple parallel pellet reactors: A model-based approach. *Water Sci. Technol.* **2006**, *53*, 493–501. [[CrossRef](#)] [[PubMed](#)]
58. van Schagen, K.; Rietveld, L.; Babuška, R.; Baars, E. Control of the fluidised bed in the pellet softening process. *Chem. Eng. Sci.* **2008**, *63*, 1390–1400. [[CrossRef](#)]
59. Ye, X.; Gao, Y.; Cheng, J.; Chu, D.; Ye, Z.-L.; Chen, S. Numerical simulation of struvite crystallization in fluidized bed reactor. *Chem. Eng. Sci.* **2018**, *176*, 242–253. [[CrossRef](#)]
60. Moguel, L.F.; Muhr, H.; Dietz, A.; Plasari, E. CFD simulation of barium carbonate precipitation in a fluidized bed reactor. *Chem. Eng. Res. Des.* **2010**, *88*, 1206–1216. [[CrossRef](#)]
61. Segev, R.; Hasson, D.; Semiat, R. Modeling CaCO₃ precipitation in fluidized bed CO₂ stripping desalination process. *Desalination* **2013**, *311*, 192–197. [[CrossRef](#)]
62. Mangold, M.; Khlopov, D.; Temmel, E.; Lorenz, H.; Seidel-Morgenstern, A. Modelling geometrical and fluid-dynamic aspects of a continuous fluidized bed crystallizer for separation of enantiomers. *Chem. Eng. Sci.* **2017**, *160*, 281–290. [[CrossRef](#)]
63. Gänsch, J.; Huskova, N.; Kerst, K.; Temmel, E.; Lorenz, H.; Mangold, M.; Janiga, G.; Seidel-Morgenstern, A. Continuous enantioselective crystallization of chiral compounds in coupled fluidized beds. *Chem. Eng. J.* **2021**, *422*, 129627. [[CrossRef](#)]
64. Godskesen, B.; Hauschild, M.; Rygaard, M.; Zambrano, K.; Albrechtsen, H.-J. Life cycle assessment of central softening of very hard drinking water. *J. Environ. Manag.* **2012**, *105*, 83–89. [[CrossRef](#)]
65. Van der Bruggen, B.; Goossens, H.; Everard, P.A.A.; Stengée, K.; Rogge, W. Cost-benefit analysis of central softening for production of drinking water. *J. Environ. Manag.* **2009**, *91*, 541–549. [[CrossRef](#)] [[PubMed](#)]
66. Beeftink, M.; Hofs, B.; Kramer, O.; Odegard, I.; van der Wal, A. Carbon footprint of drinking water softening as determined by life cycle assessment. *J. Clean. Prod.* **2021**, *278*, 123925. [[CrossRef](#)]
67. van Dijk, J.C.; Wilms, D.A. Water treatment without waste material. Fundamentals and state of the art of pellet softening. *Aqua-J. Water Supply Res. Technol.* **1991**, *40*, 263–280.
68. Kramer, O.J.I.; van Schaik, C.; Hangelbroek, J.J.; de Moel, P.J.; Colin, M.G.; Amsing, M.; Boek, E.S.; Breugem, W.P.; Padding, J.T.; van der Hoek, J.P. A novel sensor measuring local voidage profile inside a fluidised bed reactor. *J. Water Process Eng.* **2021**, *42*, 102091. [[CrossRef](#)]
69. Schippers, D.; Kooi, M.; Sjoerdsma, P.; De Bruijn, F. Colour removal by ion exchange and reuse of regenerant by means of nanofiltration. *Water Sci. Technol. Water Supply* **2004**, *4*, 57–64. [[CrossRef](#)]
70. Van Houwelingen, G.; Bond, R.; Seacord, T.; Fessler, E. Experiences with pellet reactor softening as pretreatment for inland desalination in the USA. *Desalin. Water Treat.* **2010**, *13*, 259–266. [[CrossRef](#)]
71. Hu, R.; Huang, T.; Wen, G.; Tang, Z.; Liu, Z.; Li, K. Pilot study on the softening rules and regulation of water at various hardness levels within a chemical crystallization circulating pellet fluidized bed system. *J. Water Process Eng.* **2021**, *41*, 102000. [[CrossRef](#)]
72. Tang, C.; Hedegaard, M.J.; Lopato, L.; Albrechtsen, H.-J. Softening of drinking water by the pellet reactor—Effects of influent water composition on calcium carbonate pellet characteristics. *Sci. Total Environ.* **2019**, *652*, 538–548. [[CrossRef](#)]
73. Sioson, A.S.; Choi, A.E.S.; de Luna, M.D.G.; Huang, Y.-H.; Lu, M.-C. Calcium carbonate granulation in a fluidized-bed reactor: Kinetic, parametric and granule characterization analyses. *Chem. Eng. J.* **2020**, *382*, 122879. [[CrossRef](#)]
74. Sioson, A.S.; De Luna, M.D.G.; Lu, M.-C. A kinetic study of calcium carbonate granulation through fluidized-bed homogeneous process for removal of calcium-hardness from raw and tap waters. *Adv. Sci. Technol. Innov.* **2020**, 199–201. [[CrossRef](#)]
75. Hirasawa, I.; Toya, Y. *Fluidized-Bed Process for Phosphate Removal by Calcium Phosphate Crystallization*; ACS Symposium Series; ACS Publications: Washington, DC, USA, 1990; Volume Chapter 26–438, pp. 355–363. [[CrossRef](#)]
76. Seckler, M.M.; Van Leeuwen, M.L.J.; Bruinsma, O.S.L.; Van Rosmalen, G.M. Phosphate removal in a fluidized bed—II Process optimization. *Water Res.* **1996**, *30*, 1589–1596. [[CrossRef](#)]
77. Harris, W.G.; Wilkie, A.C.; Cao, X.; Sirengo, R. Bench-scale recovery of phosphorus from flushed dairy manure wastewater. *Bioresour. Technol.* **2008**, *99*, 3036–3043. [[CrossRef](#)] [[PubMed](#)]

78. Deng, L.; Wang, Y.; Zhang, X.; Zhou, J.; Huang, T. Defluoridation by fluorapatite crystallization in a fluidized bed reactor under alkaline groundwater condition. *J. Clean. Prod.* **2020**, *272*, 122805. [CrossRef]
79. Rugaika, A.M.; Van Deun, R.; Njau, K.N.; Van der Bruggen, B. Phosphorus Recovery as Calcium Phosphate by a Pellet Reactor Pre-Treating Domestic Wastewater Before Entering a Constructed Wetland. *Int. J. Environ. Sci. Technol.* **2019**, *16*, 3851–3860. [CrossRef]
80. Battistoni, P.; De Angelis, A.; Prisciandaro, M.; Boccadoro, R.; Bolzonella, D. P removal from anaerobic supernatants by struvite crystallization: Long term validation and process modelling. *Water Res.* **2002**, *36*, 1927–1938. [CrossRef]
81. Battistoni, P.; Fava, G.; Pavan, P.; Musacco, A.; Cecchi, F. Phosphate removal in anaerobic liquors by struvite crystallization without addition of chemicals: Preliminary results. *Water Res.* **1997**, *31*, 2925–2929. [CrossRef]
82. Ohlinger, K.N.; Young, T.M.; Schroeder, E.D. Postdigestion struvite precipitation using a fluidized bed reactor. *J. Environ. Eng.* **2000**, *126*, 361–368. [CrossRef]
83. Battistoni, P. Struvite crystallization: A feasible and reliable way to fix phosphorus in anaerobic supernatants. *Water Res.* **2000**, *34*, 3033–3041. [CrossRef]
84. Battistoni, P.; De Angelis, A.; Pavan, P.; Prisciandaro, M.; Cecchi, F. Phosphorus removal from a real anaerobic supernatant by struvite crystallization. *Water Res.* **2001**, *35*, 2167–2178. [CrossRef]
85. Britton, A.; Koch, F.A.; Mavinic, D.S.; Adnan, A.; Oldham, W.K.; Udala, B. Pilot-scale struvite recovery from anaerobic digester supernatant at an enhanced biological phosphorus removal wastewater treatment plant. *J. Environ. Eng. Sci.* **2005**, *4*, 265–277. [CrossRef]
86. Ye, X.; Ye, Z.-L.; Lou, Y.; Pan, S.; Wang, X.; Wang, M.K.; Chen, S. A comprehensive understanding of saturation index and upflow velocity in a pilot-scale fluidized bed reactor for struvite recovery from swine wastewater. *Powder Technol.* **2016**, *295*, 16–26. [CrossRef]
87. Zamora, P.; Georgieva, T.; Salcedo, I.; Elzinga, N.; Kuntke, P.; Buisman, C.J.N. Long-term operation of a pilot-scale reactor for phosphorus recovery as struvite from source-separated urine. *J. Chem. Technol. Biotechnol.* **2017**, *92*, 1035–1045. [CrossRef]
88. Ye, X.; Chen, M.; Wang, W.; Shen, J.; Wu, J.; Huang, W.; Xiao, L.; Lin, X.; Ye, Z.-L.; Chen, S. Dissolving the high-cost with acidity: A happy encounter between fluidized struvite crystallization and wastewater from activated carbon manufacture. *Water Res.* **2021**, *188*, 116521. [CrossRef] [PubMed]
89. Fattah, K.P.; Mavinic, D.S.; Koch, F.A.; Jacob, C. Determining the feasibility of phosphorus recovery as struvite from filter press centrate in a secondary wastewater treatment plant. *J. Environ. Sci. Health Part A* **2008**, *43*, 756–764. [CrossRef]
90. Bhuiyan, M.I.H.; Mavinic, D.S.; Koch, F.A. Phosphorus recovery from wastewater through struvite formation in fluidized bed reactors: A sustainable approach. *Water Sci. Technol.* **2008**, *57*, 175–181. [CrossRef] [PubMed]
91. Shimamura, K.; Ishikawa, H.; Tanaka, T.; Hirasawa, I. Use of a seeder reactor to manage crystal growth in the fluidized bed reactor for phosphorus recovery. *Water Environ. Res.* **2007**, *79*, 406–413. [CrossRef]
92. Ueno, Y.; Fujii, M. Three years experience of operating and selling recovered struvite from full-scale plant. *Environ. Technol.* **2001**, *22*, 1373–1381. [CrossRef] [PubMed]
93. Crutchik, D.; Morales, N.; Vázquez-Padín, J.R.; Garrido, J.M. Enhancement of struvite pellets crystallization in a full-scale plant using an industrial grade magnesium product. *Water Sci. Technol.* **2017**, *75*, 609–618. [CrossRef]
94. Battistoni, P.; Paci, B.; Fatone, F.; Pavan, P. Phosphorus Removal from Anaerobic Supernatants: Start-Up and Steady-State Conditions of a Fluidized Bed Reactor Full-Scale Plant. *Ind. Eng. Chem. Res.* **2006**, *45*, 663–669. [CrossRef]
95. Ostara. Available online: <https://ostara.com/phosphates-production/> (accessed on 28 July 2022).
96. Siciliano, A.; Limonti, C.; Curcio, G.M.; Molinari, R. Advances in struvite precipitation technologies for nutrients removal and recovery from aqueous waste and wastewater. *Sustainability* **2020**, *12*, 7538. [CrossRef]
97. Shim, S.; Won, S.; Reza, A.; Kim, S.; Ahmed, N.; Ra, C. Design and optimization of fluidized bed reactor operating conditions for struvite recovery process from swine wastewater. *Processes* **2020**, *8*, 422. [CrossRef]
98. Chu, D.; Ye, Z.-L.; Chen, S.; Xiong, X. Comparative study of heavy metal residues in struvite products recovered from swine wastewater using fluidised bed and stirred reactors. *Water Sci. Technol.* **2018**, *78*, 1642–1651. [CrossRef] [PubMed]
99. Lee, C.-W.; Kwon, H.B.; Kim, Y.-J.; Jeon, H.-P. Nutrients recovery by struvite formation from wastewater in a fluidized bed reactor. *Mater. Sci. Forum* **2005**, *486–487*, 387–390. [CrossRef]
100. Rabinovich, A.; Rouff, A.A.; Lew, B.; Ramlogan, M.V. Aerated Fluidized Bed Treatment for Phosphate Recovery from Dairy and Swine Wastewater. *ACS Sustain. Chem. Eng.* **2018**, *6*, 652–659. [CrossRef]
101. Ryu, H.D.; Lim, D.Y.; Kim, S.J.; Baek, U.-I.; Chung, E.G.; Kim, K.; Lee, J.K. Struvite precipitation for sustainable recovery of nitrogen and phosphorus from anaerobic digestion effluents of swine manure. *Sustainability* **2020**, *12*, 8574. [CrossRef]
102. Al-Mallahi, J.; Sürmeli, R.Ö.; Çalli, B. Recovery of phosphorus from liquid digestate using waste magnesite dust. *J. Clean. Prod.* **2020**, *272*, 122616. [CrossRef]
103. Sun, H.; Hernandez, V.L.C.; Mohammed, A.N.; Liu, Y. Impact of Total Suspended Solids on Struvite Precipitation from Source-Diverted Blackwater. *J. Environ. Eng.* **2021**, *147*, 04020157. [CrossRef]
104. Shih, Y.-J.; Abarca, R.R.M.; de Luna, M.D.G.; Huang, Y.-H.; Lu, M.-C. Recovery of phosphorus from synthetic wastewaters by struvite crystallization in a fluidized-bed reactor: Effects of pH, phosphate concentration and coexisting ions. *Chemosphere* **2017**, *173*, 466–473. [CrossRef]

105. Rabinovich, A.; Heckman, J.R.; Lew, B.; Rouff, A.A. Magnesium supplementation for improved struvite recovery from dairy lagoon wastewater. *J. Environ. Chem. Eng.* **2021**, *9*, 105628. [[CrossRef](#)]
106. Meng, Y.; Li, Z.; Wang, L.; Li, Y. P-recovery as struvite from the enhanced anaerobic phosphorus release supernatant in a pilot-scale fluidized bed reactor and characterization of the product. *Chin. J. Environ. Eng.* **2021**, *15*, 1377–1385. [[CrossRef](#)]
107. Lahav, O.; Telzhensky, M.; Zewuhn, A.; Gendel, Y.; Gerth, J.; Calmano, W.; Birnhack, L. Struvite recovery from municipal-wastewater sludge centrifuge supernatant using seawater NF concentrate as a cheap Mg(II) source. *Sep. Purif. Technol.* **2013**, *108*, 103–110. [[CrossRef](#)]
108. Battistoni, P.; Pavan, P.; Cecchi, F.; Mata-Alvares, J. Effect of composition of anaerobic supernatants from an anaerobic, anoxic and oxic (A₂O) process on struvite and hydroxyapatite formation. *Ann. Chim.* **1998**, *88*, 761–772.
109. Wilsenach, J.A.; Schuurbiens, C.A.H.; van Loosdrecht, M.C.M. Phosphate and potassium recovery from source separated urine through struvite precipitation. *Water Res.* **2007**, *41*, 458–466. [[CrossRef](#)]
110. Jordaan, E.M.; Rezania, B.; Çiçek, N. Investigation of chemical-free nutrient removal and recovery from CO₂-rich wastewater. *Water Sci. Technol.* **2013**, *67*, 2195–2201. [[CrossRef](#)] [[PubMed](#)]
111. Su, C.-C.; Dulfo, L.D.; Dalida, M.L.P.; Lu, M.-C. Magnesium phosphate crystallization in a fluidized-bed reactor: Effects of pH, Mg:P molar ratio and seed. *Sep. Purif. Technol.* **2014**, *125*, 90–96. [[CrossRef](#)]
112. Hanhoun, M.; Montastruc, L.; Azzaro-Pantel, C.; Biscans, B.; Frèche, M.; Pibouleau, L. Simultaneous determination of nucleation and crystal growth kinetics of struvite using a thermodynamic modeling approach. *Chem. Eng. J.* **2013**, *215–216*, 903–912. [[CrossRef](#)]
113. Ye, Z.; Shen, Y.; Ye, X.; Zhang, Z.; Chen, S.; Shi, J. Phosphorus recovery from wastewater by struvite crystallization: Property of aggregates. *J. Environ. Sci.* **2014**, *26*, 991–1000. [[CrossRef](#)]
114. Ghosh, S.; Lobanov, S.; Lo, V.K. Impact of supersaturation ratio on phosphorus recovery from synthetic anaerobic digester supernatant through a struvite crystallization fluidized bed reactor. *Environ. Technol.* **2019**, *40*, 2000–2010. [[CrossRef](#)]
115. Fang, C.; Zhang, T.; Jiang, R.; Ohtake, H. Phosphate enhance recovery from wastewater by mechanism analysis and optimization of struvite settleability in fluidized bed reactor. *Sci. Rep.* **2016**, *6*, 32215. [[CrossRef](#)]
116. Su, C.-C.; Reano, R.L.; Dalida, M.L.P.; Lu, M.-C. Barium recovery by crystallization in a fluidized-bed reactor: Effects of pH, Ba/P molar ratio and seed. *Chemosphere* **2014**, *105*, 100–105. [[CrossRef](#)]
117. Shih, Y.-J.; Chang, H.-C.; Huang, Y.-H. Reclamation of phosphorus from aqueous solutions as alkaline earth metal phosphate in a fluidized-bed homogeneous crystallization (FBHC) process. *J. Taiwan Inst. Chem. Eng.* **2016**, *62*, 177–186. [[CrossRef](#)]
118. Bayon, L.L.E.; Ballesteros, F.C.; Choi, A.E.S.; Garcia-Segura, S.; Lu, M.C. Remediation of cobalt from semiconductor wastewater in the frame of fluidized-bed homogeneous granulation process. *J. Environ. Chem. Eng.* **2021**, *9*, 105936. [[CrossRef](#)]
119. Lacson, C.F.Z.; Lu, M.-C.; Huang, Y.-H. Chemical precipitation at extreme fluoride concentration and potential recovery of CaF₂ particles by fluidized-bed homogenous crystallization process. *Chem. Eng. J.* **2021**, *415*, 128917. [[CrossRef](#)]
120. Deng, L.; Zhang, X.; Huang, T.; Zhou, J. Investigation of fluorapatite crystallization in a fluidized bed reactor for the removal of fluoride from groundwater. *J. Chem. Technol. Biotechnol.* **2019**, *94*, 569–581. [[CrossRef](#)]
121. Dominguez-Ramos, A.; Aldaco, R.; Irabien, A. Life Cycle Assessment as a Tool for Cleaner Production: Application to Aluminium Trifluoride. *Int. J. Chem. React. Eng.* **2007**, *5*. [[CrossRef](#)]
122. Aldaco, R.; Irabien, A.; Luis, P. Fluidized bed reactor for fluoride removal. *Chem. Eng. J.* **2005**, *107*, 113–117. [[CrossRef](#)]
123. Van den Broeck, K.; Van Hoornick, N.; Van Hoeymissen, J.; de Boer, R.; Giesen, A.; Wilms, D. Sustainable treatment of HF wastewaters from semiconductor industry with a fluidized bed reactor. *IEEE Trans. Semicond. Manuf.* **2003**, *16*, 423–428. [[CrossRef](#)]
124. Aldaco, R.; Garea, A.; Irabien, A. Fluoride Recovery in a Fluidized Bed: Crystallization of Calcium Fluoride on Silica Sand. *Ind. Eng. Chem. Res.* **2006**, *45*, 796–802. [[CrossRef](#)]
125. Jiang, K.; Zhou, K.G. Recovery and removal of fluoride from fluorine industrial wastewater by crystallization process: A pilot study. *Clean Technol. Environ. Policy* **2017**, *19*, 2335–2340. [[CrossRef](#)]
126. Aldaco, R.; Garea, A.; Fernández, I.; Irabien, A. Resources reduction in the fluorine industry: Fluoride removal and recovery in a fluidized bed crystallizer. *Clean Technol. Environ. Policy* **2008**, *10*, 203–210. [[CrossRef](#)]
127. Segev, R.; Hasson, D.; Semiat, R. Improved high recovery brackish water desalination process based on fluidized bed air stripping. *Desalination* **2011**, *281*, 75–79. [[CrossRef](#)]
128. Li, C.-W.; Jian, J.-C.; Liao, J.-C. Integrating membrane filtration and a fluidized-bed pellet reactor for hardness removal. *J. Am. Water Work. Assoc.* **2004**, *96*, 151–158. [[CrossRef](#)]
129. Nefzi, M.; Amor, M.B.; Maâlej, M. A clean technology for decarbonation of geothermal waters from Chott El Fejje using a three-phase fluidized bed reactor-Modelling aspects. *Desalination* **2004**, *165*, 337–350. [[CrossRef](#)]
130. Hu, R.; Liu, Z.; Huang, T.; Wen, G. Pilot test of simultaneous removal of silica, hardness, and turbidity from gray water using circulating pellet fluidized bed. *J. Water Process Eng.* **2021**, *42*, 102149. [[CrossRef](#)]
131. Lv, X.; Li, J.; Chen, H.; Tang, H. Copper wastewater treatment with high concentration in a two-stage crystallization-based combined process. *Environ. Technol.* **2018**, *39*, 2346–2352. [[CrossRef](#)] [[PubMed](#)]
132. Costodes, V.C.T.; Lewis, A.E. Reactive crystallization of nickel hydroxy-carbonate in fluidized-bed reactor: Fines production and column design. *Chem. Eng. Sci.* **2006**, *61*, 1377–1385. [[CrossRef](#)]
133. Lee, C.-I.; Yang, W.-F.; Hsieh, C.-I. Removal of Cu(II) from aqueous solution in a fluidized-bed reactor. *Chemosphere* **2004**, *57*, 1173–1180. [[CrossRef](#)]

134. Lertratwattana, K.; Kemacheevakul, P.; Garcia-Segura, S.; Lu, M.-C. Recovery of copper salts by fluidized-bed homogeneous granulation process: High selectivity on malachite crystallization. *Hydrometallurgy* **2019**, *186*, 66–72. [[CrossRef](#)]
135. Wei, Z.; Xiong, Y.; Chen, J.; Bai, J.; Wu, J.; Zuo, J.; Wang, K. Recovery of Cu(II) from aqueous solution by induced crystallization in a long-term operation. *J. Environ. Sci.* **2018**, *69*, 183–191. [[CrossRef](#)]
136. Bayon, L.L.E.; Ballesteros, F.C.; Garcia-Segura, S.; Lu, M.-C. Water reuse nexus with resource recovery: On the fluidized-bed homogeneous crystallization of copper and phosphate from semiconductor wastewater. *J. Clean. Prod.* **2019**, *236*, 117705. [[CrossRef](#)]
137. Ballesteros, F.C.; Salcedo, A.F.S.; Vilando, A.C.; Huang, Y.-H.; Lu, M.-C. Removal of nickel by homogeneous granulation in a fluidized-bed reactor. *Chemosphere* **2016**, *164*, 59–67. [[CrossRef](#)] [[PubMed](#)]
138. Chen, J.P.; Yu, H. Lead removal from synthetic wastewater by crystallization in a fluidized-bed reactor. *J. Environ. Sci. Health Part A Toxic/Hazard. Subst. Environ. Eng.* **2000**, *35*, 817–835. [[CrossRef](#)]
139. Hoang, M.T.; Pham, T.D.; Nguyen, V.T.; Nguyen, M.K.; Pham, T.T.; Van der Bruggen, B. Removal and recovery of lead from wastewater using an integrated system of adsorption and crystallization. *J. Clean. Prod.* **2019**, *213*, 1204–1216. [[CrossRef](#)]
140. De Luna, M.D.G.; Bellotindos, L.M.; Asiao, R.N.; Lu, M.-C. Removal and recovery of lead in a fluidized-bed reactor by crystallization process. *Hydrometallurgy* **2015**, *155*, 6–12. [[CrossRef](#)]
141. Udomkitthawewat, N.; Anotai, J.; Choi, A.E.S.; Lu, M.C. Removal of zinc based on a screw manufacturing plant wastewater by fluidized-bed homogeneous granulation process. *J. Clean. Prod.* **2019**, *230*, 1276–1286. [[CrossRef](#)]
142. Vilando, A.C.; Caparanga, A.R.; Lu, M.-C. Enhanced recovery of aluminum from wastewater using a fluidized bed homogeneously dispersed granular reactor. *Chemosphere* **2019**, *223*, 330–341. [[CrossRef](#)]
143. Wilms, D.; Vercaemst, K.; Van Dijk, J.C. Recovery of silver by crystallization of silver carbonate in a fluidized-bed reactor. *Water Res.* **1992**, *26*, 235–239. [[CrossRef](#)]
144. Tsevis, A.; Sotiropoulou, M.; Koutsoukos, P.G. Preparation of titania powders in a fluidized-bed reactor. *Prog. Colloid Polym. Sci.* **2000**, *115*, 151–155. [[CrossRef](#)]
145. Zhou, P.; Huang, J.-C.; Li, A.W.; Wei, S. Heavy metal removal from wastewater in fluidized bed reactor. *Water Res.* **1999**, *33*, 1918–1924. [[CrossRef](#)]
146. Lee, C.-I.; Yang, W.-F. Heavy Metal Removal from Aqueous Solution in Sequential Fluidized-Bed Reactors. *Environ. Technol.* **2005**, *26*, 1345–1354. [[CrossRef](#)] [[PubMed](#)]
147. Chung, J.; Jeong, E.; Choi, J.W.; Yun, S.T.; Maeng, S.K.; Hong, S.W. Factors affecting crystallization of copper sulfide in fed-batch fluidized bed reactor. *Hydrometallurgy* **2015**, *152*, 107–112. [[CrossRef](#)]
148. Huang, C.; Pan, J.R.; Lee, M.; Yen, S. Treatment of high-level arsenic-containing wastewater by fluidized bed crystallization process. *J. Chem. Technol. Biotechnol.* **2007**, *82*, 289–294. [[CrossRef](#)]
149. Lewis, A.E.; Swartbooi, A. Factors Affecting Metal Removal in Mixed Sulfide Precipitation. *Chem. Eng. Technol.* **2006**, *29*, 277–280. [[CrossRef](#)]
150. De Luna, M.D.G.; Rance, D.P.M.; Bellotindos, L.M.; Lu, M.-C. A statistical experimental design to remove sulfate by crystallization in a fluidized-bed reactor. *Sustain. Environ. Res.* **2017**, *27*, 117–124. [[CrossRef](#)]
151. De Luna, M.D.G.; Rance, D.P.M.; Bellotindos, L.M.; Lu, M.-C. Removal of sulfate by fluidized bed crystallization process. *J. Environ. Chem. Eng.* **2017**, *5*, 2431–2439. [[CrossRef](#)]
152. Seewoo, S.; Van Hille, R.; Lewis, A.E. Aspects of gypsum precipitation in scaling waters. *Hydrometallurgy* **2004**, *75*, 135–146. [[CrossRef](#)]
153. Maharaj, C.; Chivavava, J.; Lewis, A.E. Treatment of a highly-concentrated sulphate-rich synthetic wastewater using calcium hydroxide in a fluidised bed crystallizer. *J. Environ. Manag.* **2018**, *207*, 378–386. [[CrossRef](#)] [[PubMed](#)]
154. Halevy, S.; Korin, E.; Gilron, J. Kinetics of Gypsum Precipitation for Designing Interstage Crystallizers for Concentrate in High Recovery Reverse Osmosis. *Ind. Eng. Chem. Res.* **2013**, *52*, 14647–14657. [[CrossRef](#)]
155. Vu, X.; Lin, J.-Y.; Shih, Y.-J.; Huang, Y.-H. Reclaiming Boron as Calcium Perborate Pellets from Synthetic Wastewater by Integrating Chemical Oxo-Precipitation within a Fluidized-Bed Crystallizer. *ACS Sustain. Chem. Eng.* **2018**, *6*, 4784–4792. [[CrossRef](#)]
156. Tsai, C.-K.; Lee, N.-T.; Huang, G.-H.; Suzuki, Y.; Doong, R. Simultaneous Recovery of Display Panel Waste Glass and Wastewater Boron by Chemical Oxo-precipitation with Fluidized-Bed Heterogeneous Crystallization. *ACS Omega* **2019**, *4*, 14057–14066. [[CrossRef](#)]
157. Le, V.G.; Vo, T.D.H.; Nguyen, B.S.; Vu, C.T.; Shih, Y.J.; Huang, Y.H. Recovery of iron(II) and aluminum(III) from acid mine drainage by sequential selective precipitation and fluidized bed homogeneous crystallization (FBHC). *J. Taiwan Inst. Chem. Eng.* **2020**, *115*, 135–143. [[CrossRef](#)]
158. De Luna, M.D.G.; Sioson, A.S.; Choi, A.E.S.; Abarca, R.R.M.; Huang, Y.-H.; Lu, M.-C. Operating pH influences homogeneous calcium carbonate granulation in the frame of CO₂ capture. *J. Clean. Prod.* **2020**, *272*, 1222325. [[CrossRef](#)]
159. Guillard, D.; Lewis, A.E. Optimization of nickel hydroxycarbonate precipitation using a laboratory pellet reactor. *Ind. Eng. Chem. Res.* **2002**, *41*, 3110–3114. [[CrossRef](#)]
160. Guillard, D.; Lewis, A.E. Nickel carbonate precipitation in a fluidized-bed reactor. *Ind. Eng. Chem. Res.* **2001**, *40*, 5564–5569. [[CrossRef](#)]
161. Mamoad, R.Y.; Caparanga, A.R.; Choi, A.E.S.; Lu, M.-C. Remediation of oxalate in a homogeneous granulation process in the frame of crystallization. *Chem. Eng. Commun.* **2022**, *209*, 378–389. [[CrossRef](#)]

162. Guevara, H.P.R.; Ballesteros, F.C.; Vilando, A.C.; de Luna, M.D.G.; Lu, M.-C. Recovery of oxalate from bauxite wastewater using fluidized-bed homogeneous granulation process. *J. Clean. Prod.* **2017**, *154*, 130–138. [[CrossRef](#)]
163. Caddarao, P.S.; Garcia-Segura, S.; Ballesteros, F.C., Jr.; Huang, Y.-H.; Lu, M.-C.; Ballesteros, F.C.; Huang, Y.-H.; Lu, M.-C. Phosphorous recovery by means of fluidized bed homogeneous crystallization of calcium phosphate. Influence of operational variables and electrolytes on brushite homogeneous crystallization. *J. Taiwan Inst. Chem. Eng.* **2018**, *83*, 124–132. [[CrossRef](#)]
164. Li, X.; Hasson, D.; Semiat, R.; Shemer, H. Intermediate concentrate demineralization techniques for enhanced brackish water reverse osmosis water recovery—A review. *Desalination* **2019**, *466*, 24–35. [[CrossRef](#)]
165. Tran, A.T.K.; Zhang, Y.; Jullok, N.; Meesschaert, B.; Pinoy, L.; Van der Bruggen, B. RO concentrate treatment by a hybrid system consisting of a pellet reactor and electro dialysis. *Chem. Eng. Sci.* **2012**, *79*, 228–238. [[CrossRef](#)]
166. Sobhani, R.; Abahusayn, M.; Gabelich, C.J.J.; Rosso, D. Energy Footprint analysis of brackish groundwater desalination with zero liquid discharge in inland areas of the Arabian Peninsula. *Desalination* **2012**, *291*, 106–116. [[CrossRef](#)]
167. Li, C.-W.; Liao, J.-C.; Lin, Y.-C. Integrating a membrane and a fluidized pellet reactor for removing hardness: Effects of NOM and phosphate. *Desalination* **2005**, *175*, 279–288. [[CrossRef](#)]
168. Kohli, H.; Emmermann, D.; Kadaj, R.; Said, H. Hybrid desalting technology maximizes recovery. *Desalination* **1985**, *56*, 61–68. [[CrossRef](#)]
169. Chen, Y.; Davis, J.R.J.R.; Nguyen, C.H.C.H.; Baygents, J.C.J.C.; Farrell, J. Electrochemical Ion-Exchange Regeneration and Fluidized Bed Crystallization for Zero-Liquid-Discharge Water Softening. *Environ. Sci. Technol.* **2016**, *50*, 5900–5907. [[CrossRef](#)] [[PubMed](#)]
170. Liu, K.; Huang, Q.; Long, X.; Cao, Z.; Zhou, B. RO concentrate softening through induced crystallization in a fluidized bed reactor. *MATEC Web Conf.* **2016**, *49*, 04003. [[CrossRef](#)]
171. Tran, A.T.K.; Mondal, P.; Lin, J.; Meesschaert, B.; Pinoy, L.; Van der Bruggen, B. Simultaneous regeneration of inorganic acid and base from a metal washing step wastewater by bipolar membrane electro dialysis after pretreatment by crystallization in a fluidized pellet reactor. *J. Membr. Sci.* **2015**, *473*, 118–127. [[CrossRef](#)]
172. Tran, A.T.K.; Zhang, Y.; De Corte, D.; Hannes, J.-B.; Ye, W.; Mondal, P.; Jullok, N.; Meesschaert, B.; Pinoy, L.; Van Der Bruggen, B. P-recovery as calcium phosphate from wastewater using an integrated selectrodialysis/crystallization process. *J. Clean. Prod.* **2014**, *77*, 140–151. [[CrossRef](#)]
173. Sluys, J.T.M.; Verdoes, D.; Hanemaaijer, J.H. Water treatment in a Membrane-Assisted Crystallizer (MAC). *Desalination* **1996**, *104*, 135–139. [[CrossRef](#)]
174. Lee, C.; Yang, W.; Chiou, C. Utilization of water clarifier sludge for copper removal in a liquid fluidized-bed reactor. *J. Hazard. Mater.* **2006**, *129*, 58–63. [[CrossRef](#)]
175. Lyu, C.; Zhou, D.; Wang, J. Removal of multi-dye wastewater by the novel integrated adsorption and Fenton oxidation process in a fluidized bed reactor. *Environ. Sci. Pollut. Res.* **2016**, *23*, 20893–20903. [[CrossRef](#)]
176. Anotai, J.; Sakulkittimasak, P.; Boonrattanakij, N.; Lu, M.-C. Kinetics of nitrobenzene oxidation and iron crystallization in fluidized-bed Fenton process. *J. Hazard. Mater.* **2009**, *165*, 874–880. [[CrossRef](#)]
177. Cai, Q.Q.; Wu, M.Y.; Hu, L.M.; Lee, B.C.Y.; Ong, S.L.; Wang, P.; Hu, J.Y. Organics removal and in-situ granule activated carbon regeneration in FBR-Fenton/GAC process for reverse osmosis concentrate treatment. *Water Res.* **2020**, *183*, 116119. [[CrossRef](#)] [[PubMed](#)]
178. Bello, M.M.; Abdul Raman, A.A.; Asghar, A. Fenton oxidation treatment of recalcitrant dye in fluidized bed reactor: Role of SiO₂ as carrier and its interaction with fenton's reagent. *Environ. Prog. Sustain. Energy* **2019**, *38*, 13188. [[CrossRef](#)]
179. Burhenne, L.; Giacomini, C.; Follett, T.; Ritchie, J.; McCahill, J.S.J.; Mérida, W. Characterization of reactive CaCO₃ crystallization in a fluidized bed reactor as a central process of direct air capture. *J. Environ. Chem. Eng.* **2017**, *5*, 5968–5977. [[CrossRef](#)]
180. Giacomini, C.E.; Holm, T.; Mérida, W. CaCO₃ growth in conditions used for direct air capture. *Powder Technol.* **2020**, *370*, 39–47. [[CrossRef](#)]
181. Papirio, S.; Villa-Gomez, D.K.; Esposito, G.; Pirozzi, F.; Lens, P.N.L. Acid Mine Drainage Treatment in Fluidized-Bed Bioreactors by Sulfate-Reducing Bacteria: A Critical Review. *Crit. Rev. Environ. Sci. Technol.* **2013**, *43*, 2545–2580. [[CrossRef](#)]
182. Kaksonen, A.H.; Puhakka, J.A. Sulfate Reduction Based Bioprocesses for the Treatment of Acid Mine Drainage and the Recovery of Metals. *Eng. Life Sci.* **2007**, *7*, 541–564. [[CrossRef](#)]
183. Qamar, S.; Galan, K.; Peter Elsner, M.; Hussain, I.; Seidel-Morgenstern, A. Theoretical investigation of simultaneous continuous preferential crystallization in a coupled mode. *Chem. Eng. Sci.* **2013**, *98*, 25–39. [[CrossRef](#)]
184. Vetter, T.; Burcham, C.L.; Doherty, M.F. Separation of conglomerate forming enantiomers using a novel continuous preferential crystallization process. *AIChE J.* **2015**, *61*, 2810–2823. [[CrossRef](#)]
185. Temmel, E.; Gänsch, J.; Seidel-Morgenstern, A.; Lorenz, H. Systematic investigations on continuous fluidized bed crystallization for chiral separation. *Crystals* **2020**, *10*, 394. [[CrossRef](#)]
186. Kerst, K.; de Souza, L.M.; Bartz, A.; Seidel-Morgenstern, A.; Janiga, G. CFD-DEM simulation of a fluidized bed crystallization reactor. *Comput. Aided Chem. Eng.* **2015**, *37*, 263–268. [[CrossRef](#)]
187. Binev, D.; Seidel-Morgenstern, A.; Lorenz, H. Continuous Separation of Isomers in Fluidized Bed Crystallizers. *Cryst. Growth Des.* **2016**, *16*, 1409–1419. [[CrossRef](#)]
188. Soh, S.H.; Lee, L.Y. Microencapsulation and nanoencapsulation using supercritical fluid (SCF) techniques. *Pharmaceutics* **2019**, *11*, 21. [[CrossRef](#)]

189. Niu, F.; Subramaniam, B. Particle Fluidization with Supercritical Carbon Dioxide: Experiments and Theory. *Ind. Eng. Chem. Res.* **2007**, *46*, 3153–3156. [[CrossRef](#)]
190. Tsutsumi, A.; Nakamoto, S.; Mineo, T.; Yoshida, K. A novel fluidized-bed coating of fine particles by rapid expansion of supercritical fluid solutions. *Powder Technol.* **1995**, *85*, 275–278. [[CrossRef](#)]
191. Leeke, G.A.; Lu, T.; Bridson, R.H.; Seville, J.P.K. Application of nano-particle coatings to carrier particles using an integrated fluidized bed supercritical fluid precipitation process. *J. Supercrit. Fluids* **2014**, *91*, 7–14. [[CrossRef](#)]
192. Li, Q.; Huang, D.; Lu, T.; Seville, J.P.K.; Xing, L.; Leeke, G.A. Supercritical fluid coating of API on excipient enhances drug release. *Chem. Eng. J.* **2017**, *313*, 317–327. [[CrossRef](#)]
193. Matos, R.L.; Lu, T.; McConville, C.; Leeke, G.; Ingram, A. Analysis of curcumin precipitation and coating on lactose by the integrated supercritical antisolvent-fluidized bed process. *J. Supercrit. Fluids* **2018**, *141*, 143–156. [[CrossRef](#)]
194. Matos, R.L.; Lu, T.; Leeke, G.; Prosapio, V.; McConville, C.; Ingram, A. Single-step coprecipitation and coating to prepare curcumin formulations by supercritical fluid technology. *J. Supercrit. Fluids* **2020**, *159*, 104758. [[CrossRef](#)]
195. Chen, T.; Liu, L.; Zhang, L.; Lu, T.; Matos, R.L.; Jiang, C.; Lin, Y.; Yuan, T.; Ma, Z.; He, H.; et al. Optimization of the supercritical fluidized bed process for sirolimus coating and drug release. *Int. J. Pharm.* **2020**, *589*, 119809. [[CrossRef](#)]